8-12-2009

Microplasma MEMS device: its design, fabrication and application in hydrogen generation for fuel cells

BinduMadhav Sabnavis

Microplasma MEMS device: Its design, fabrication and application in hydrogen generation for fuel cells

by

Sabnavis BinduMadhav

A Thesis Submitted in Partial Fulfillment of the Requirements for the Degree

of

Master of Science

in

Materials Science and Engineering

Approved by:

Professor: Dr. Yen-Wen Lu (Thesis Advisor)

Professor: Dr. Gerald Takacs (Thesis Committee Member)

Professor: Dr. K.S.V. Santhanam (Department Chair, Thesis Committee Member)

CENTER FOR MATERIAL SCIENCE AND ENGINEERING

COLLEGE OF SCIENCE

ROCHESTER INSTITUTE OF TECHNOLOGY

ROCHESTER, NEW YORK

AUGUST 12, 2009

Abstract

Devices capable of generating microscale plasma (microplasma) were designed, fabricated and characterized. The microplasma was employed to disassociate hydrogen from hydrogen-constituent gases. The devices were designed such that the Ignition Voltage of plasma was low, at atmospheric pressure and non thermal in nature. The devices were tested while Argon (Ar) or Helium (He) was used as carrier gas. Two designs were conceived: a coplanar device and a parallel plate electrode device. The current-voltage (I-V) relationship and optical emission spectra (OES) characteristics were collected for the two designs with both gases. A fuel cell was used to verify the hydrogen generation from this process. Finally, a coil design for testing RF-powered device was fabricated and tested under original conditions. All of the results, fabrication methods and plasma analysis are explained.

I dedicate this master's thesis:

To my parents, Murali & Uma Sabnavis ,who are the reason where I stand

To my brothers, Giridhar & Shashidhar, who are ever present for supporting me

To all the teachers who didn't give up on me and taught me many different things

To all the friends from my childhood to present who made life an exciting adventure

Acknowledgements

I am grateful and thankful to my advisor Dr. Wen-Yen Lu, for providing me with the opportunity to work on next generation technology, encouragement, guidance, ideas, support and enthusiasm throughout this thesis work. I am indebted to him for providing helpful hints and suggestions at various stages of my work.

I would also like to extend my gratitude to my thesis committee members, Dr. Gerald Takacs and Dr. K. S. V. Santhanam.

I would like to thank the staff at the Semiconductor & Microsystems Fabrication Laboratory (SMFL) at RIT for their assistance in helping set up various instruments and tools for experiments. Specially, I would like to thank Sean O'Brien, SMFL process engineer, for helping with tools and process issues. I would also like to thank Thomas Grimsley (fab manager for approving materials and providing various things as and when required), John Nash, Rich Battaglia, Scott Blondell, David Yackoff and Bruce Tolleson.

I am also grateful to all of my friends and fellow graduate students, CK Chen, Michael Pepen, Rakesh Kumar Dhull, Zhonghua Yao, Cao Liang, Xiang Li, Karthik Narayanan and Yusuke Takahashi in the Micro and Nano Fabrication Laboratory at RIT for the joyful environment and the support they have given me at various stages of this project.

Table of Contents

Abstract ii
Table of Contents v
List of Tables vi
List of Figures vi
Chapter 1 - Introduction 1
1.1 Hydrogen Reforming 2
1.1.1 Thermal/Steam Process 3
1.1.2 Electrolytic Process 4
1.1.3 Photolytic Process 7
1.1.4 Plasma Reforming 8
1.2 Plasma 9
1.3 Ionization States 12
1.4 Breakdown of Gases in Electric Fields 13
1.5 Plasma Characterization 14
1.6 What is Microplasma 15
1.7 Microplasma MEMS Devices 16
1.8 Microplasma for Hydrogen Generation 18
1.9 Thesis Outline 19
Chapter 2 Devices Design, and Fabrication 20
2.1 Tools, and Materials 20
2.2 Coplanar Electrode Device 22
2.2.1 Design 22
2.2.2 Fabrication 23
2.3 Parallel Plate Electrode Device 26
2.3.1 Design 26
2.3.2 Fabrication 27
2.4 Device Design for RF Supply 30
2.4.1 Design 30
2.4.2 Fabrication 30
Chapter 3 - Characterization of Microplasma MEMS Device 32
3.1 DC Setup for I-V Characterization 32
3.2 Optical Emission Spectroscopy and Hydrogen Generation Set Up 33
3.2.1 OES 34
3.3 Fuel Cell Voltage Test Setup 37
3.4 OES Data 39
3.5 Fuel Cell Analysis 42

Chapter 4 - RF Design and Results 48
4.1 First Attempt: Coplanar and Parallel-Plate Electrode Devices for RF Microplasma 49
4.2 The Second Attempt: Coil Design 49
4.2.1 Device Design 49
4.2.2 Fabrication 51
4.3 Process Development 52
Chapter 5 - Conclusion and Future Work 54
5.1 Conclusion 54
References 56
Appendix 59

List of Tables

Table 1-1: Different Plasma Reformer Efficiencies [26] 8
Table 3-1: I-V Data at Different Flow Rates for Parallel Plate Device 45
Table 3-2: I-V Data at Different Flow Rates for Coplanar Device 46

List of Figures

Figure 1-1: Steam Reforming 4
Figure 1-2: Electrolytic Reforming [4] 5
Figure 1-3: High Temperature Electrolysis [5] 6
Figure 1-4: Photolytic Reforming 7
Figure 1-5: Dynamic Discharge in a Sliding Arc Non-Thermal Plasma Reactor (Copyright Elsevier) [26] 9
Figure 1-6: DC Plasma and Its Regions [9] 11
Figure 1-7: Range of Plasma [10] 11
Figure 1-8: Paschen Curves [11] 14
Figure 1-9: Current-Voltage Characteristics of Discharge [13] 15
Figure 1-10: a) Microplasma Device Regions Based on Gap and Electron Density b) Pressure Dependence of Electron Temperature (T_e) & Gas Temperature (T_g) [14] 16
Figure 1-11: Electrode Configurations for DBD Design [17] 17
Figure 1-12: ICP-Type Microplasma Jet Driven by VHF (450 MHz) Source [18] 17
Figure 1-13: ICP Device [19] 18
Figure 1-14: Plasma Reforming 18
Figure 2-1: Diagram of Coplanar Device 23
Figure 2-2: Coplanar Device Process Flow 25
Figure 2-3: Coplanar Device After Process (left) and Its Final Packaging (right) 25
Figure 2-4: Schematic of Parallel Plate-Electrode Device 26
Figure 2-5: Parallel Plate Device Process Flow 29
Figure 2-6: Photograph of the Fabricated Device 29
Figure 2-7: RF Design 30
Figure 2-8: Processing Steps for RF Design, Electroplating Setup 31
Figure 2-9: Gold Electroplating and Final Device 31
Figure 3-1: Schematic DC Test Setup 33
Figure 3-2: Schematic of Setup for Hydrogen Generation 34
Figure 3-3: OES Spectrometer Schematic [20] 35
Figure 3-4: OES Output 36

Figure 3-5: OES Peaks for Argn and Helium 36
Figure 3-6: Fuel Cell Test Setup 37
Figure 3-7: Image of Test Setup 38
Figure 3-8: I-V Plot for Parallel Plate Device with Argon & Helium 38
Figure 3-9: Spectra of Argon Plasma for Parallel Plate Device 39
Figure 3-10: Spectra of Helium Plasma for Parallel Plate Device 40
Figure 3-11: I-V Plot for Coplanar Device with Argon & Helium 40
Figure 3-12: Spectra of Argon Plasma for Coplanar Device 41
Figure 3-13: Spectra of Helium Plasma for Coplanar Device 41
Figure 3-14: Fuel Cell Voltage Test for Coplanar Device with Argon 42
Figure 3-15: Fuel Cell Voltage Test for Coplanar Device with Helium 42
Figure 3-16: Fuel Cell Voltage Test for Coplanar Device with Argon & Helium 43
Figure 3-17: Argon Flow at 40, 70, 100 sccm Respectively for Parallel Plate Device 44
Figure 3-18: Helium 40, 70, 100 sccm Respectively for Parallel Plate Device 44
Figure 3-19: Argon Flow at 40, 70 and 100sccm for Coplanar Device 46
Figure 3-20: Helium Flow at 40, 70 and 100sccm for Coplanar Device 46
Figure 3-21: Plasma with Argon and Helium Gas in Parallel Plate Device 47
Figure 3-22: Plasma with Argon and Helium Gas in Coplanar Device 47
Figure 4-1: RF Device Test Setup 48
Figure 4-2: RF Plasma & After Effects 49
Figure 4-3: RF Plasma Device [19] 50
Figure 4-4: Gold Electroplating 51
Figure 4-5: Process Development 52
Figure 4-6: c) Electroplating on Gold Substrate with SU 8 Mold 52
Figure 4-7: RF Device 53
Figure 4-8: RF Device After Testing 53
Figure A-1: Process Flow for Parallel Plate Device with AZ9260 Resist 59
Figure A-2: Process Flow for Parallel Plate Device with SU 8 Resist 59
Figure A-3: Relative Humidity to Absolute Humidity Conversion Chart 60
Figure A-4: SU 8 Resist Speed vs. Thickness Plot 61
Figure A-5: AZ9260 Resist Speed vs. Thickness Plot 61

Chapter 1 - Introduction

The rise in global energy demand, combined with depleting reserves of fossil fuels and environmental considerations, have increased interest in alternative sources of energy with hydrogen fuel being one of the alternatives. At present, hydrogen generation (hydrogen reforming) mostly resorts to thermo-chemical conversion [1,2] − an energy intensive, but inefficient process. The reaction occurs at the catalytic surface and not in the whole reformer chamber. Plasma-based reformers can offer a great advantage and potential for hydrogen generation, in which volume reactivity exists and energy coupling is controlled through the application of electromagnetic fields, thereby reducing energy dissipation. Storage of hydrogen using conventional methods is not efficient. A gram of hydrogen gas occupies about 11 liters (2.9 gallons) of space at atmospheric pressure. For convenience, the gas must be intensely pressurized to several hundred atmospheres then stored in a pressure vessel. In liquid form, hydrogen can only be stored under cryogenic temperatures. Thus, generating hydrogen from constituent gases as and when required solves storage and transportation issues. Hydrogen fuel for mobile applications is a topic being widely researched. The ability to generate hydrogen as and when required by convenient means make hydrogen fuel safe and convenient. This chapter discusses, in brief, the technique of hydrogen reforming with different processes on a large scale as well as the research being made to miniaturize the process and research being done in microplasma devices.

1.1 Hydrogen Reforming

Hydrogen is a colorless and odorless gas. It is sparingly soluble in water and the solubility is not affected by change of temperature. It is a better conductor of heat than other gases, with its conductivity being about five times that of air. It reacts chemically with most elements; forms compounds with a large number of elements; and in many cases, compounds are formed by the direct combination of the elements

Hydrogen demand, at present, is met by hydrogen production from fossil fuels. Most of the refineries are located in remote areas. The hydrogen produced must be delivered to the users either by truck or via hydrogen pipelines. Due to the inherently low energy density of hydrogen, transportation by truck is not a viable option. Hydrogen delivery using pipelines is not cost-effective either because of the high cost of the pipelines. Therefore, hydrogen production for a future hydrogen economy is likely to be accomplished using a distributed system, where hydrogen is generated as and when required.

Hydrogen production in a large scale by separating hydrogen from low-density hydrocarbons is known as *steam reforming*, with steam and high pressure being utilized for enabling the process. It is a thermo-chemical conversion; that is, an energy-intensive and inefficient process with the conversion taking place on the catalytic surface rather than in the whole reformer chamber. The following are some popular techniques used for hydrogen reforming:

a) Thermal process (heat treatment of hydrogen constituent gases and hydrocarbons)

b) Electrolytic process (breakdown of water using electricity)

c) Photolytic process (use of light energy to split water),

d) Plasma reforming.

1.1.1 Thermal/Steam Process

Steam reforming converts hydrocarbons such as methane present in natural gas into hydrogen and carbon monoxide by reaction with steam over a metal catalyst (commonly nickel). This process accounts most of the hydrogen generated at present. There are four main steps involved in hydrogen steam reforming. They are:

1. **Reformation of Natural Gas** - The first step of the process involves natural gas reacting with steam at 750-800°C (1380-1470ºF) to produce a synthesis gas (syngas), a mixture primarily made up of hydrogen (H_2) and carbon monoxide (CO).

$$CH_4 + H_2O \rightarrow CO + 3\ H_2 \qquad (1.1)$$

2. **Shift Reaction** - In the second step, known as water gas shift (WGS) reaction, the carbon monoxide produced in the first reaction reacts with steam over a catalyst (e.g. nickel) to form hydrogen and carbon dioxide (CO_2). This process occurs in two stages, consisting of a high temperature shift (HTS) at 350ºC (662ºF) and a low temperature shift (LTS) at 190-210ºC (374-410ºF).

$$CO + H_2O \rightarrow CO_2 + H_2 \qquad (1.2)$$

Hydrogen produced by steam reforming process includes small quantities of carbon monoxide, carbon dioxide, and hydrogen sulfide as impurities and, depending on use, may require further purification. The primary steps for purification include Feedstock Purification and Product Purification.

3. **Feedstock Purification** - This step removes poisons, including sulfur (S) and chloride (Cl), to increase the life of the downstream steam reforming and other catalysts.

4. **Product Purification** - This step removes CO_2 in a liquid absorption system. The product gas undergoes a methanation step to remove residual traces of carbon oxides. Newer SMR plants utilize a pressure swing absorption (PSA) unit instead, producing 99.99% pure product hydrogen.

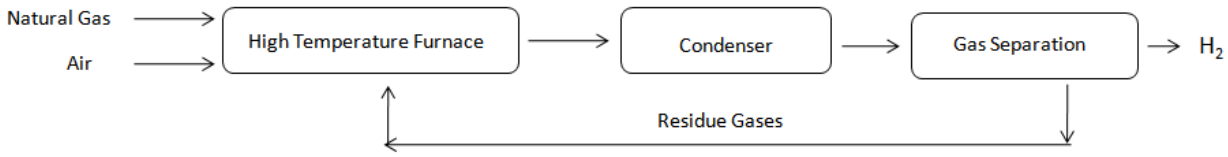

Figure 1-1: Steam Reforming

Coal Gasification, Biomass Gasification, and Natural Gas Reforming all use similar techniques for hydrogen generation. Steam process is the most efficient process (85%-90%) for large scale hydrogen production [3].

1.1.2 Electrolytic Process

Conventional electrolysis uses only electric current to separate hydrogen from water, whereas high-temperature electrolysis enhances the efficiency of the process by adding substantial external heat (high-temperature steam). A high-temperature system has the potential to achieve overall conversion efficiencies of 45–50%, compared to approximately 30% for conventional electrolysis [4]. Commercial low temperature electrolyzers have system efficiencies of 56–73% (70.1–53.4 kWh/kg hydrogen at 1 atmosphere and 25 ^{o}C).

The technology of hydrogen production through conventional water electrolysis is well-established. As shown in Figure 1-2, electrolysis splits water into its components—hydrogen and oxygen—by charging water with an electrical current. The charge breaks the chemical bond

between the hydrogen and oxygen and splits apart the atomic components. The resulting ions form at two poles: the *anode*, which is positively charged, and the *cathode*, which is negatively charged. Hydrogen ions gather at the cathode and react with it to form hydrogen gas, which is then collected. Oxygen goes through a similar process at the anode. The below stated are the standard reactions.

Anode Reaction: $2H_2O \rightarrow O_2 + 4H^+ + 4e^-$ (1.3)

Cathode Reaction: $4H^+ + 4e^- \rightarrow 2H_2$ (1.4)

The main drawbacks of conventional electrolysis for large-scale hydrogen production are the amount of electricity required for the process and the high cost of membrane production.

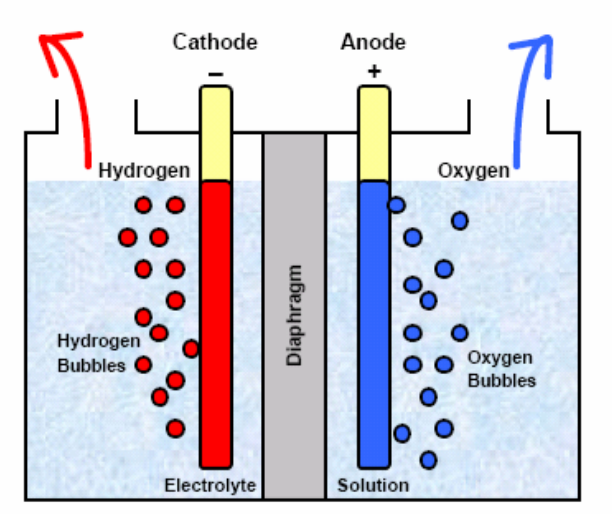

Figure 1-2: Electrolytic Reforming [4]

To reduce the required high electricity in electrolysis, High-Temperature Electrolysis (HTE) adds in some of the energy needed to split the water as heat instead of electricity; thus, reducing the overall energy required. HTE uses a device similar to a Solid Oxide Fuel Cell (SOFC).

As shown in Figure 1-3, the electrolytic cell essentially consists of a solid oxide electrolyte with conducting electrodes deposited on either side of the electrolyte. A mixture of steam and hydrogen at 750-950ºC is supplied to the anode side of the electrolyte. Oxygen ions are drawn through the electrolyte by the electrical potential and combine to oxygen on the cathode side. The steam-hydrogen mixture exits and the water and hydrogen gas mixture are passed through a separator to separate hydrogen.

The high-temperature system uses heat directly rather than converting heat to electricity, increasing efficiency. This direct use of heat is based on assumption that a readily-available, non fossil-fuel-based source of high heat is available. Advantages for high temperature electrolysis with a solid oxide based electrolyzer include the use of a solid electrolyte, which, is non-corrosive and does not experience any liquid and flow distribution problems [5].

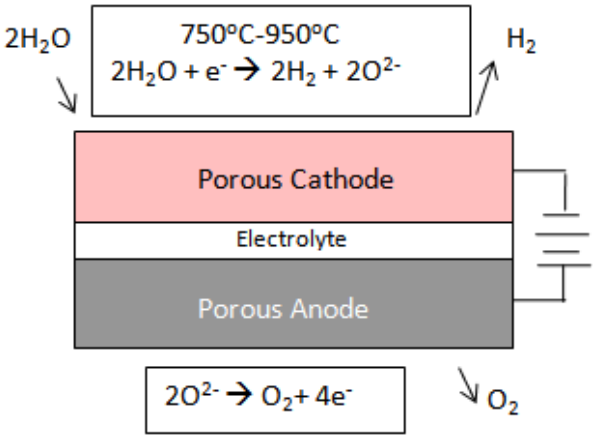

Figure 1-3: High Temperature Electrolysis [5]

1.1.3 Photolytic Process

The conversion of solar energy into useful energy forms can generally be divided into thermal and photonic processes. In *solar thermal processes*, solar energy is first converted to heat, which can either be used directly and stored in a thermal medium (e.g., water or dry rocks) or converted to mechanical and/or electrical energy by an appropriate machine (e.g., a steam turbine for the generation of electricity). In *solar photonic processes*, the solar photons are absorbed directly into an absorber, with little heat conversion. The absorber may convert parts of the photon energy to electricity (as in a photovoltaic cell), or store part as chemical energy in an endergonic chemical reaction (as in photosynthesis or the conversion of water to hydrogen and oxygen). Figure 1-4 shows typical process for hydrogen generation using sunlight. [7]

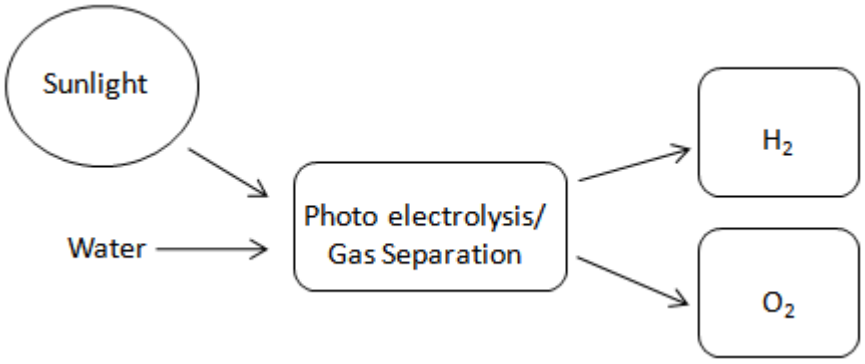

Figure 1-4: Photolytic Reforming

The other type of photo electrolysis is where a *photocathode*, a p-type material with excess holes, or a *photo anode*, an n-type of material with excess electrons, is immersed in an aqueous electrolyte rather than generating an electric current, where water is split to form hydrogen and oxygen. The oxygen and hydrogen gasses are separated, for example, by the use of a semi-permeable membrane [8].

Electrolytic and Photolytic processes are incapable of generating hydrogen in large quantities. Steam reforming can generate large amounts of hydrogen. Generation of large quantities is not required for mobile applications. All of the three processes are inefficient for small scale hydrogen generation.

1.1.4 Plasma Reforming

In *plasma reforming*, the overall reforming reactions are the same as conventional reforming; however, energy and free radicals used for the reforming reaction are provided by plasma typically generated with electricity or heat [21-22]. Plasma has sufficient energy to split hydrogen containing molecules such as water. When water or steam is injected with the fuel, H, OH, and O radicals in addition to electrons are formed, and create conditions for both reductive and oxidative reactions to occur [23].

Plasmas can be configured to operate at lower temperatures than traditional reforming [22, 24, 25]. In the cases where no catalysts are used to assist the reforming, the process is highly sulfur tolerant [22, 24, 25]. The main reported disadvantages include the electrical requirements and high electrode erosion at elevated pressures [27].

Technology	Fuel	Experimental Conditions			Products (dry vol.%)				Reformate Temperature (K)	Efficiency, η
		Chemical Reaction	Air Ratio	S/C	H_2	CO	CO_2	CH_4		
Gliding arc non-thermal	Diesel	ATR	0.4	1.8	23	17	6.2	1.2	1000–1300	85
Corona discharge + catalyst	Iso-octane	ATR	0.28	1	46	16	16	–	900–1100	55
Gliding arc thermal	Iso-octane	POx	0.25	–	22	15	2	3	1200	9
Gliding arc thermal	Diesel	POx	0.25	–	23.5	23	0.1	0.03	1200	9
Microwave	Hexane	SR	–	2	66	25	4	–	?	?

Table 1-1: Different Plasma Reformer Efficiencies [26]

Gliding arc plasma, dielectric barrier discharge (DBD), microwave plasma, and corona discharge are four types of non-thermal plasma. The first three types use dynamic discharge to create the plasma while the corona discharge generates the plasma with a static discharge. The

gliding arc plasma has two diverging electrodes. An arc is formed where the gas enters by applying a high voltage. The gas pushes the arc down the length of the reactor. As the gas reaches the end of the reactor, the arc is turned off. Another arc is then formed at the gas entrance. The DBD reactor is typically an annular configuration. The gases flow in a small gap between the high-voltage electrode encased in a non-conductive material such as quartz, with the outer shell being the ground electrode. This process creates hydrogen. We found that when a pure methane feed is used, carbon black and a plasma polymerized carbon film are produced [28].

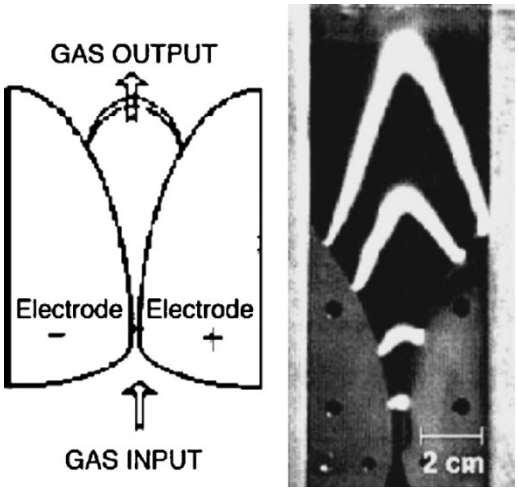

Figure 1-5: Dynamic Discharge in a Sliding Arc Non-Thermal Plasma Reactor (Copyright Elsevier) [26]

1.2 Plasma

It is known that there are four states in which matter can exist. The commonly know three states are Solid, Liquid, and Gaseous. The fourth state is Plasma. In *Solid state,* all the molecules are tightly packed in either a repeated pattern or otherwise. In this state the matter has a fixed shape, which can be changed only by the influence of external factors (heat, pressure etc). In the *Liquid state*, all the molecules have very little interaction between one another. There is no pattern in which the molecules are arranged. Liquids take the shape of the container (water,

alcohol eg). In the *Gaseous state*, molecules are independent of interactions, with each molecule independent from one other. The molecules are in random motion and occupy any empty space. When gases are compressed, they start to repel from one another (Air, Helium) and apply pressure on the enclosing region.

Plasma has well-defined regions. Plasma discharges evolve through four regions with increasing electric field strength, or voltage gradient (volts per meter), between the negative cathode and positive anode. Transitions from one region to another can be abrupt, with millivolts separating different regions [9]. Plasma is generally generated between oppositely charged electrodes and in a low pressure gaseous medium. There are several distinct plasma regions between the electrodes. As shown in Figure 1-6, the first region is the *Cathode Dark Space* starting from cathode side and is a relatively dark region with a strong electric field, a positive space charge, and a relatively high ion density. The second region is the *Negative Glow*, which has the brightest intensity of the entire discharge. Electrons accelerated in the cathode region to high speeds produce ionization while slower electrons with inelastic collisions produce excitations. The negative glow is generated by the slow electrons. The third region is the *Farady Dark Space.* It is a region of non-fluorescence that extends from the cathode for a distance dependent mainly on the gas pressure and fourth region is the positive column. Here the bright region is caused by charged particles that have a low net charge density. The electric field is just large enough to maintain the degree of ionization to reach the anode

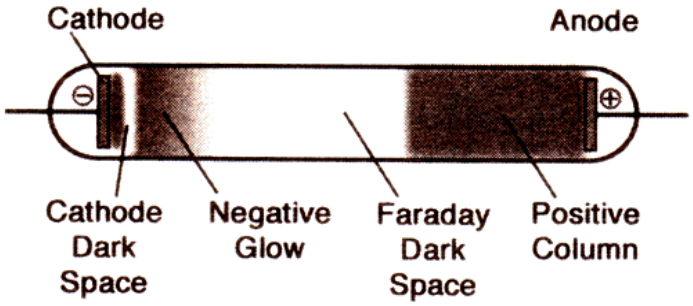

Figure 1-6: DC Plasma and Its Regions [9]

Plasma is an ionized gas; where free positive charges, negative charges, and neutral species co-exist. The Plasma state can exist over a wide range as shown in Figure 1-7 and can conduct electricity and interact strongly with electric and magnetic fields.

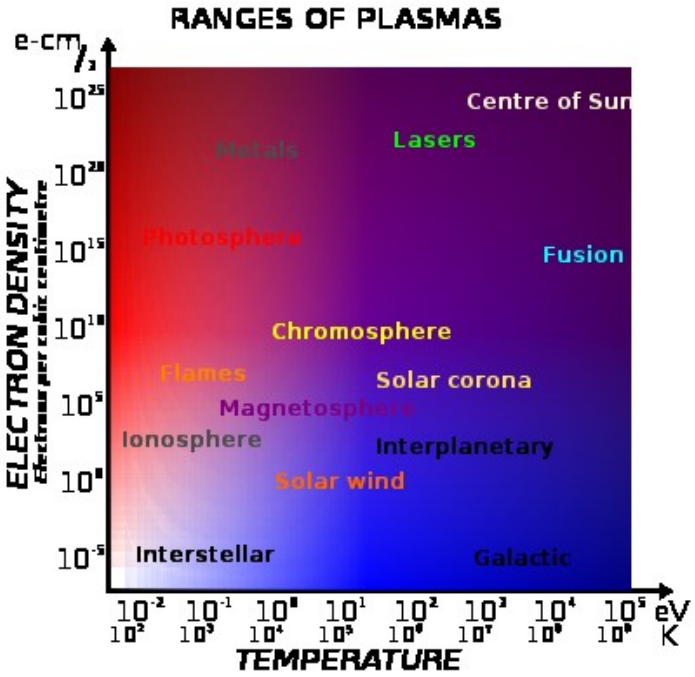

***Figure 1-7: Range of Plasma** [10]*

Providing energy for producing electron-ion pairs generates plasma. Plasma is present everywhere in the universe. The ionization degree in plasma can be defined as:

$$DI = n_e/N, \tag{1.5}$$

where n_e and N are the number densities of electrons and neutral species, respectively.

1.3 Ionization States

The application of a potential difference between a pair of electrodes produces plasma discharges. The pressure and type of gas are the other determinants. When a gas is exposed to high electrical potential, the partial ionization of the gas takes place. Collisions between electrical charges and other particles induce the ionization of bound electrons with the consequent formation of free electrons and positively charged particles. The ionization of an atom is expressed as follows:

The ionization is expressed as follows:

$$e^- + A \rightarrow A^+ + 2e^- \tag{1.6}$$

Ionization of molecules molecule ion formation:

$$e^- + AB \rightarrow AB^+ + 2e^- \tag{1.7}$$

Dissociative ionization and fragment ion formation:

$$e^- + A + B \rightarrow A + B^+ + 2e^- \tag{1.8}$$

Dissociative ionization and ion pair formation:

$$e^- + AB \rightarrow A^+ + B^+ + 3e^- \tag{1.9}$$

where A and B represent two different species. The above steps can be summarized as basic ionization processes.

In plasmas, atoms and ions are promoted to higher energy levels by absorbing energy. When the excited particles relax from higher energy level (E_q) to lower energy level (E_p), they emit radiation at specific wavelengths. The wavelengths are dependent on the levels of the transitions involved. The wavelength (λ) is related to the frequency (ν) and the energies (E_q, E_p) of the atomic levels (q, p) between which the transition takes place and is expressed as:

$$hv_{qp} = hc / \lambda_{qp} = Eq - Ep \tag{1.10}$$

where, c is the speed of light and h is the Planck constant.

1.4 Breakdown of Gases in Electric Fields

Gas breakdown is fundamentally a threshold course of action. This means breakdown only occurs when the field exceeds a value characterizing a specific set of conditions. The breakdown voltage, or ignition potential, V_t depends on the gas components, the material of the cathode, the pressure, and the discharge gap width [11].

The uniform-field breakdown in most gases is described by the Paschen's law, which relates the breakdown voltage (Vt) to the product of pressure (p) with distance (d).

Paschen Law's is as follow:

$$Vt = \frac{\text{Bpd}}{\ln(\text{Apd}) - \ln\left[\ln\left(1+\frac{1}{\gamma}\right)\right]} \tag{1.11}$$

where V_t is the ignition potential, A and B are constants, that depend on the gas being used; γ is the secondary electron emission coefficient for the cathode [11, 12].

Before the ignition potential is reached, a very small current exists while the voltage across the discharge gap is gradually increased. Ionization avalanche process occurs at a certain value of voltage, the ignition potential. At this point, the current sharply increases and light emission is observed.

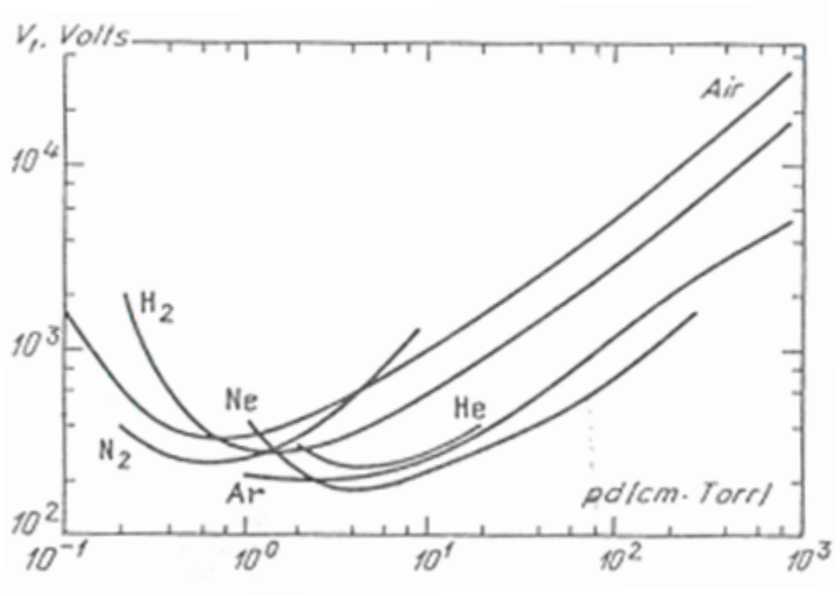

Figure 1-8: Paschen Curves [11]

1.5 Plasma Characterization

Plasma has distinct properties that can be plotted (Figure 1-9). There are three main regions: dark, glow, and arc discharges. The first being is the dark discharge, or Townsend, region where the electric field is high enough for the electrons present in gas to acquire sufficient energy to ionize a neutral atom creating more free charged particles and this process multiplies. This is called the *avalanche process*. Glow Discharge is the region where plasma gas emits light because the electron energy and number density are high enough to generate excited gas atoms by collisions. The excited gas atoms eventually relax to their ground state by emission of photons and finally Arc Discharge is the region of electrical breakdown of a gas, which produces an ongoing plasma discharge resulting from a current flowing through normally nonconductive media such as air.

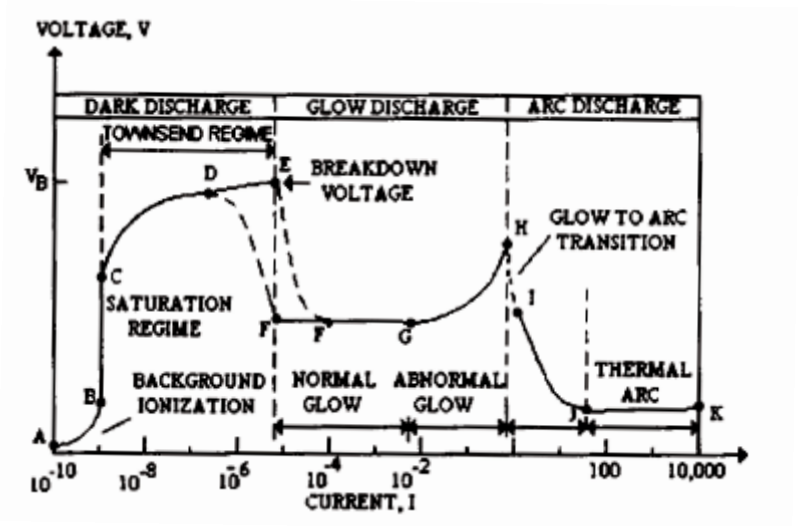

Figure 1-9: Current-Voltage Characteristics of Discharge [13]

1.6 What is Microplasma

Continuing to follow Paschen's law, microplasma takes advantage of the product of pressure and electrode gap which determines the plasma voltage. The gap can be reduced to microscale for plasma to be generated at atmospheric pressure. Microplasma has reactive, radiative, conductive and dielectric properties inherently.

Microplasmas are usually functional at high-pressure, including atmospheric pressure, and have the characteristics that are not similar to low pressure plasmas because of different operating conditions and the miniature feature size. These new properties can be used along with the more traditional properties of plasma for design and application in many fields such as nano-material syntheses, micromachining tools, microchemical analyses, photonic devices, and biomaterial processing [14].

Figure 1-10a shows the types of devices being researched upon and how the gap between electrodes and electron density are related. Figure 1.10b shows how pressure determines the electron and gas temperature.

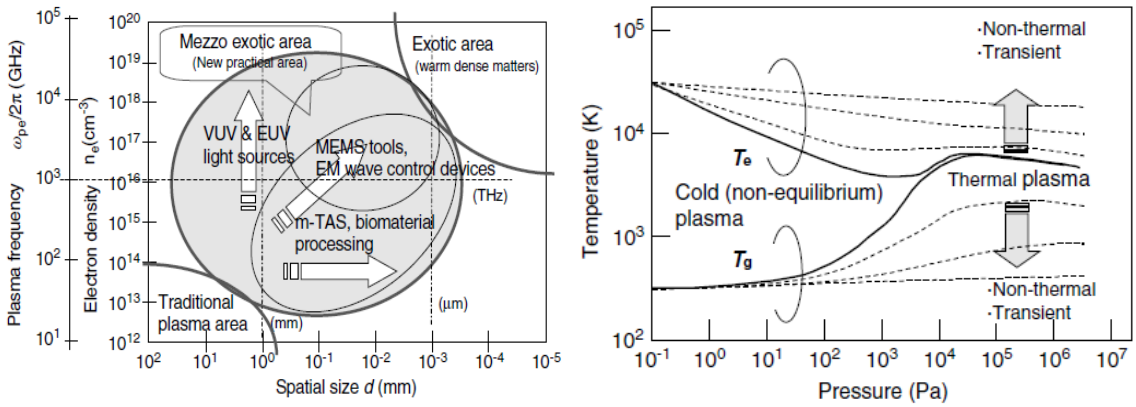

a) b)

Figure 1-10: a) Microplasma Device Regions Based on Gap and Electron Density b) Pressure Dependence of Electron Temperature (T_e) & Gas Temperature (T_g) [14]

1.7 Microplasma MEMS Devices

There are numerous ways of generating microplasma. The main requirements being a carrier gas, a power supply (DC, RF, PDC, MW), and gap between electrodes. All these things determine the microplasma. One of the designs is the Hollow Cathode design developed by Schoenbach's (Figure 1-18) group for miniaturized structures and integrated assemblies. Their design is a simple metal–insulator–metal structure with a through-hole of hundreds micrometers in diameter. It allowed electrons to perform a pendulum motion in the cathode area for increasing the ionization rate, which is called the hollow cathode effect [15, 16].

The dielectric barrier discharge (DBD) configuration is shown in Figure 1-12. In this figure, at least one and sometimes both of the electrodes are covered with an insulating material. The unit cell of a current commercial plasma display panel (PDP) is an example. There are many configurations of devices that are fabricated based on requirement [17].

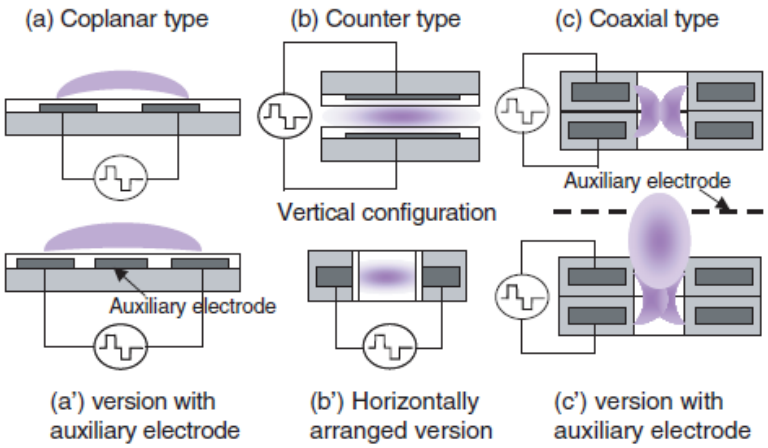

Figure 1-11: Electrode Configurations for DBD Design [17]

A 450 MHz power source is used in an Inductively Coupled Plasma (ICP) configuration. It has a thin tungsten wire coaxially in a quartz tube, making the ignition easier and helps in the discharge maintenance with the thermionic electron emission. The Figure 1-13 shows the image [18].

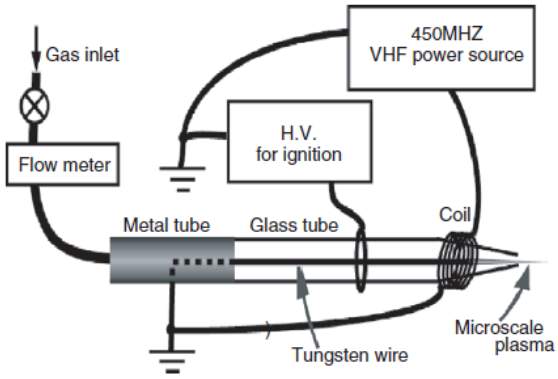

Figure 1-12: ICP-Type Microplasma Jet Driven by VHF (450 MHz) Source [18]

Dr. J. Hopwood's research group at Northeastern University has presented a ring resonator strip line is used to match the impedance with the plasma load produced at a slit in the ring, RF power supply sustained plasma with Argon as carrier gas and a pressure of 8torras shown in Figure 1-14 [19].

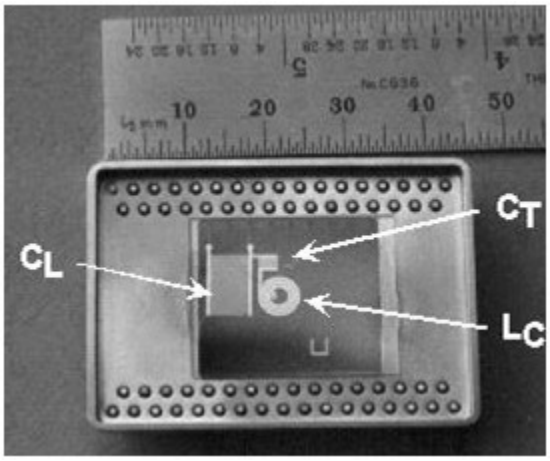

Figure 1-13: ICP Device [19]

1.8 Microplasma for Hydrogen Generation

All the present technologies deal with hydrogen generation at a large scale and then transportation as required. The idea behind our project is to generate hydrogen based on requirement. To achieve this plasma on a microscale is promising with such devices designed.

Reformer-like devices used for disassociating constituent gases to obtain hydrogen are proposed and tested. The resultant hydrogen can be used in fuel cell for generating energy.

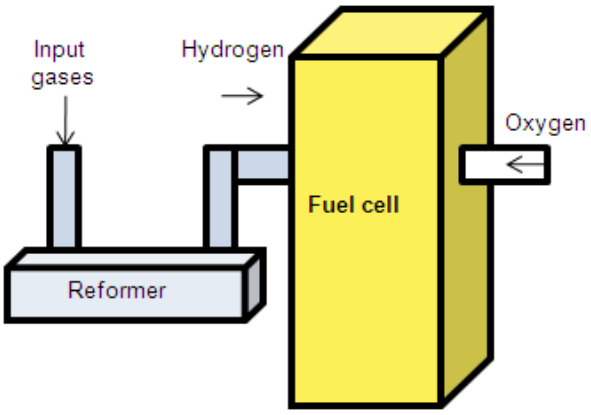

Figure 1-14: Plasma Reforming

1.9 Thesis Outline

The thesis presents the various aspects of the project in defined sections.

- Chapter 1 briefly explains about hydrogen generation and other aspects related to fuel cells functioning.
- Chapter 2 explains in detail the fabrication processes and materials used for all the different microplasma devices fabricated. The step by step process flow is explained.
- Chapter 3 is a summary of all the data collected. It has current voltage curves, OES spectra data and flow rate analysis for DC supply testing with Argon and Helium carrier gas. The hydrogen disassociated was used in fuel cell and analyzed.
- Chapter 4 explains about the RF testing results and the new coil design.
- Chapter 5 concludes all the results from different sections and discusses the future work for the project.

Chapter 2 Devices Design, and Fabrication

This chapter discusses about the devices made and material used for this project. The fabrication process steps for each of the three devices (coplanar, parallel plate, and RF device design respectively) are presented. The procedures are explained step by step.

2.1 Tools, and Materials

The following are the materials and tools used throughout this thesis and are based on stated requirements:

1. Substrates used: this section explains about the substrates and requirements taken into consideration.

   a) ITO-coated microscope slides (SPI brand, 70-100 ohms 3in by 1in by 1mm).

      Requirements: transparency of plasma region for detection and characterization

   b) Gold Coated microscope slides (Sigma Aldrich 100 Ang gold with 20 Ang Titanium seed layer, 3in by 1in by 1mm).

      Requirements: good adhesion to gold ions during electroplating

   c) Glass slides coated with Aluminum, clear 3in by 2in glass, with aluminum sputtered

      Requirements: coplanar device, good resistance to high power.

2. Resists used: this section explains about the resists and requirements taken into consideration.

   a) HPR 504 positive resist.

      Requirements: good chemical & heat resistance

      Developer for resist: Rohm & Haas CD 26 containing Tetra Methyl Ammonium Hydroxide

   b) SU 8 2010, SU 8 2050, SU 8 2035 negative resists (Microchem)

      Requirements: good chemical & heat resistance, thick resist coating, high contrast. Developer for resist: Microchem SU 8 developer containing 1-Methoxy-2-propyl acetate

   c) AZ 9260 positive resist (AZ materials)

      Requirements: good chemical & heat resistance, thick resist coating, high contrast Developer for resist: AZ400K developer containing potassium borates

3. Other Solvents Used:

   Other common solvents like de-ionized water, acetone, isopropyl alcohol; aluminum and chrome etchants were utilized during fabrication processes.

   Transene Gold electrolyte containing potassium gold cyanide and potassium cyanide was used for electroplating of gold. Transene GE-8110 and GE-8111 Gold etchant containing potassium iodide and iodine (KI/I_2) was used for etching gold.

4. Other Tools Used:

The following is a list of tools used. These are available in any IC fabricating facilities. The tools were in a cleanroom environment.

a) Karl Suss MA-55 Expose Aligner: Broad wavelength UV exposure.

b) SCS spin coater: Manually programmable spin coater. (Model: SCS P6708)

c) Kepco-DC supply range from 0-2000V and 0-2mA.

d) Function generator from 10Hz to 10MHz

e) Tokyo-Hy 13.56 MHz supply with output from 0-75W.

f) Ocean optics HR4000 optical emission spectrometer.

g) Argon, Helium & water vapor for plasma and hydrogen generation.

h) 1mm thick diamond tipped drill bits.

2.2 Coplanar Electrode Device

2.2.1 Design

In a coplanar device, the electrodes are on the same plane. The gap between them determines the plasma ignition voltage. There are some issues with peeling of film after etching. Ensuring a clean slide before sputtering of Aluminum resolves this issue.

To create a controlled gap between two electrodes for plasma generation, the coplanar device was designed. Figure 2-1 shows the design and layout of the coplanar device. The electrodes are on the same plane and the electrode gap (d) was the distance between the electrodes. The smallest gap was 20μm. Other dimensions, including 3μm, 500 μm, 250 μm and 100 μm, were tested. The electrodes were sealed with double sided tape (3M MMM137 Scotch Double Sided Tape, 3/4" Double-Sided Foam Tape) and glass slide. The glass slide had inlet and

outlet holes. The holes were drilled with a drill bit of 1mm thickness. A 1cm long by 0.5cm diameter brass hose was used as connector for gas flow.

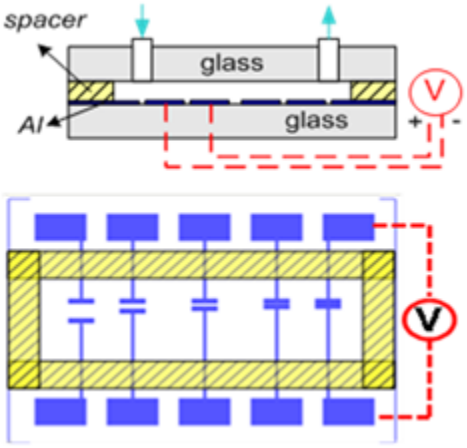

Figure 2-1: Diagram of Coplanar Device

2.2.2 Fabrication

This section explains the fabrication process of coplanar device and the processes flow for making parallel electrode device is illustrated in Figure 2-2.

1. **Clean:** 3in by 2in glass slides were rinsed a few times with acetone followed by Isopropyl alcohol (IPA) and de-ionized water (DIW).

2. **Metal Deposition:** An aluminum film of 1.2µm was sputtered by using CVC 601. The aluminum target power was 2000W, argon gas flow rate was 20sccm and the pressure of sputter chamber was below 5E-5torr. The deposition rate was 390 Å/min.

3. **Photoresist Coating:** The slides were coated with HPR-504 resist. The thickness was 1.2um. Photoresist was coated on SCS spin coater. The spin program used is shown in Appendix.

4. **Bake:** The resist coated slides were baked at 115^0C for 1 minute to remove solvents.

5. **Exposure:** The resist coated slides were exposed by using Karl Suss MA-55 contact aligner. The exposure time was set at 15sec. hard contact lithography was performed. The energy of lamp was 8mW/cm^2. The dose for exposure was approximately 1.5 times silicon substrate.

6. **Resist Development:** The exposed slides were developed in CD-26 for 45 seconds. This was done in a Petri dish.

7. **Etch Process of Electrode:** Aluminum was etched with etchant from by J.T. Baker Company. The Solution was a mixture of phosphoric, acetic, nitric acids and water (16:1:1:2). The etch rate was dependent on temperature of the etch solution. The etch rate of the solution at 50°C was 5000 Å/min. The etching was inspected visually.

8. **Sample Clean:** The slides were rinsed with acetone followed by IPA and de-ionized water (DIW).

9. **Seal and Packaging:** The slides were sealed with a 2inx1in glass slide with double sided tape. The sealing glass had two 1mm diameter holes drilled for gas inlet/outlet.

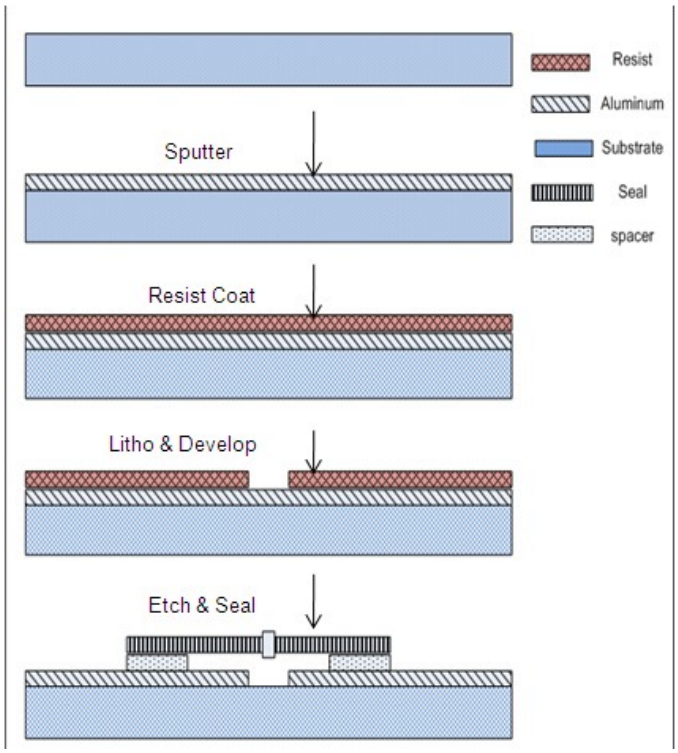

Figure 2-2: Coplanar Device Process Flow

Figure 2-3 shows the device with and without packaging.

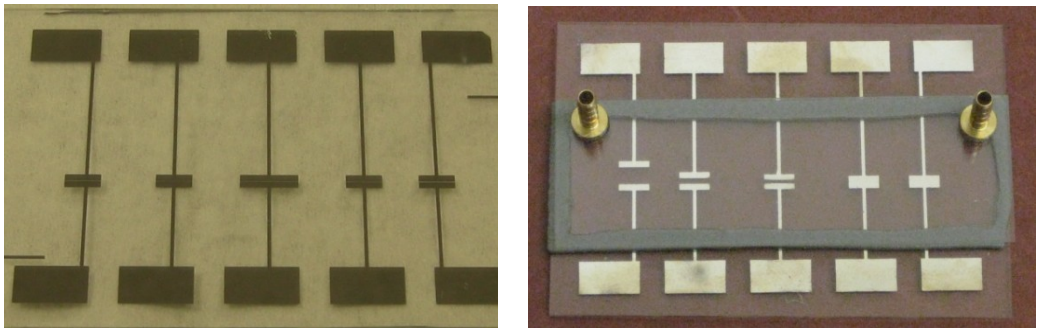

Figure 2-3: Coplanar Device After Process (left) and Its Final Packaging (right)

2.3 Parallel Plate Electrode Device

2.3.1 Design

The second design was parallel plate design. In this design two ITO coated slides were used as shown in Figure 2-4, they were spaced by photoresist. The bottom ITO slide was patterned and etched while the top layer was coated with photoresist which acted as spacer between electrodes and formed gas flow channel. Some problems faced included uneven resist coat, improper etching of ITO. The uneven coat and etching issues were solved by improving the process flow.

Figure 2-4 shows the design and layout of the coplanar device. The electrodes are on the same plane and the electrode gap (d) is the spacing between the electrodes. The smallest gap is 20µm. Other gaps, including 75µm, 50µm, 40µm and 30 m, are tested. The top electrode slide had inlet and outlet holes are drilled with a 1mm diameter drill bit.

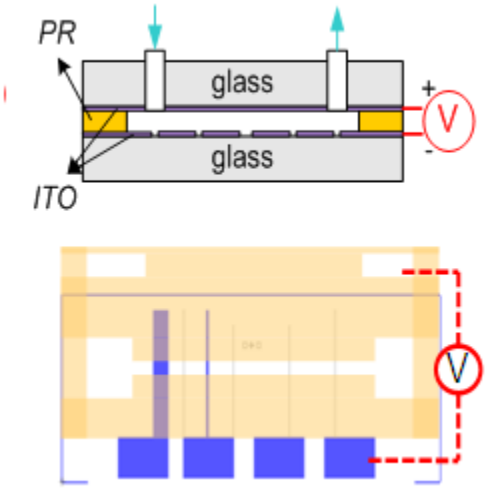

Figure 2-4: Schematic of Parallel Plate-Electrode Device

2.3.2 Fabrication

Processes flow for making parallel plate-electrode device was detailed in Figure 2-5 and explained as follows:

Part A-Bottom Electrode Processing:

1. **Clean:** ITO microscope slides (1in by 3in) were rinsed with acetone followed by IPA and DI water.
2. **Resist Bake:** the slides were baked at 115^0C for 1 minute to remove any moisture.
3. **Resist Coating:** the cleaned slides were coated with HPR-504 resist. The thickness was 1.2um. Photoresist was coated on SCS spin coater. Appendix has process flow details.
4. **Exposure:** the coated slides were exposed by using Karl Suss MA-55 contact aligner. The exposure time was set at 15sec.
5. **Resist Development:** The exposed slides were developed in CD-26 for 45 seconds. This was done in a Petri dish.
6. **Etch Process of ITO Electrodes:** This was used for etching ITO. The etch rate was dependant on HCl and H_20 ratio. A solution was prepared in such a proportion such that the etch time was 2 minutes. A new etch rate was determined each time a new lot of ITO slides was received; even when the type and manufacturer was same. The ratios used for SPI brand ITO unpolished 70-100 ohms was three parts of HCl: one part of water for first lot.

Part B-Top Electrode Processing Steps.

The below steps are for the resist developed slide of parallel electrode device with negative/positive resist, this was creating gas flow channel:

1. **Clean:** ITO microscope slides (1in by 3in) were scribed after determining the ITO side. These scribed slides were cleaned with acetone followed by IPA and de-ionized (DI) water.
2. **Bake:** the slides were baked at 95^0C for 1 minute.
3. **Resist Coating:** The cleaned slides were coated with SU 8 2010, 2015, 2050 resists. The thickness was varied from 12um to 150um. Photoresist was coated on SCS coater. The curve to show the relationship between speed and thickness can be found in Appendix.
4. **Exposure:** The coated slides were exposed on Karl Suss MA-55 contact aligner. The exposure time was varied from 60 seconds to 160 seconds based on the thickness of resist. The dose was around 1000mj/cm^2.
5. **Post Exposure Bake:** The substrates were baked at 115°C for 7-12 minutes, depending on the thickness.
6. **Resist Development:** The exposed slides were developed in SU 8 developer from 45 seconds.

SU 8 is a negative resist, in which unexposed regions clear off during development. SU 8 2000 series resist provide a thick resist coating ranging from 2-200 μm thick. AZ9260 provides coating in the range 4-25 μm

The aim was to achieve plasma ignition at lower part of Paschen curve for Argon/Helium by changing the electrode gap. AZ9260 positive resist and various SU8 negative resists were processed for finding the optimum resist. The process steps were the same for

AZ9260. AZ400K developer was the only different solution used for development of resist. Figure 2-5 shows the overall process.

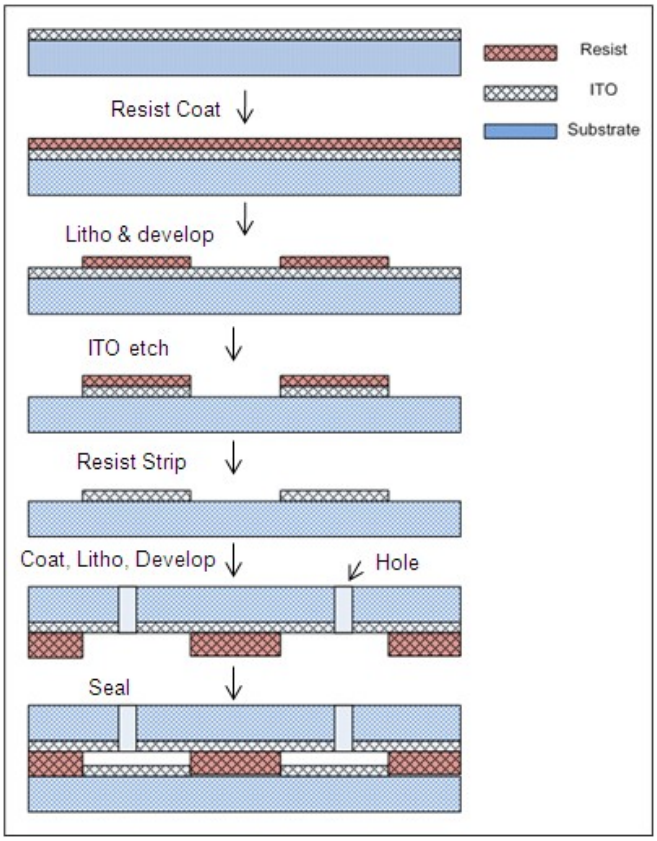

Figure 2-5: Parallel Plate Device Process Flow

Figure 2-6 shows the parallel plate device before and after packaging. The slides were sealed with double sided tapes with the ITO electrodes facing each other.

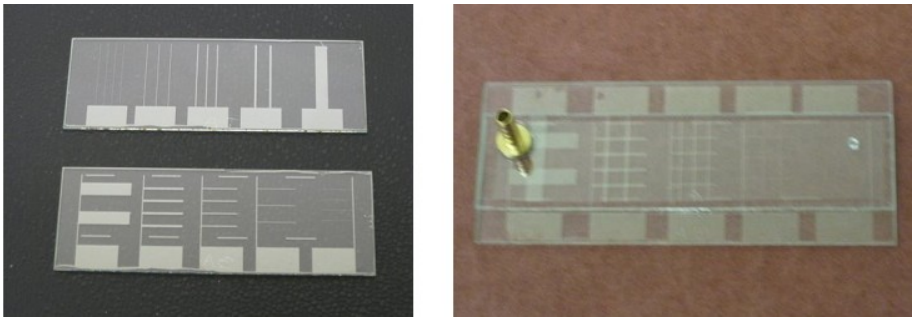

Figure 2-6: Photograph of the Fabricated Device

2.4 Device Design for RF Supply

2.4.1 Design

A new design for RF plasma was conceived with its fabrication process developed. The reasons for the new design are explained in Chapter 3. The main problem faced was deposition of thick film on glass substrate. The film was peeling off, electroplating was the solution.

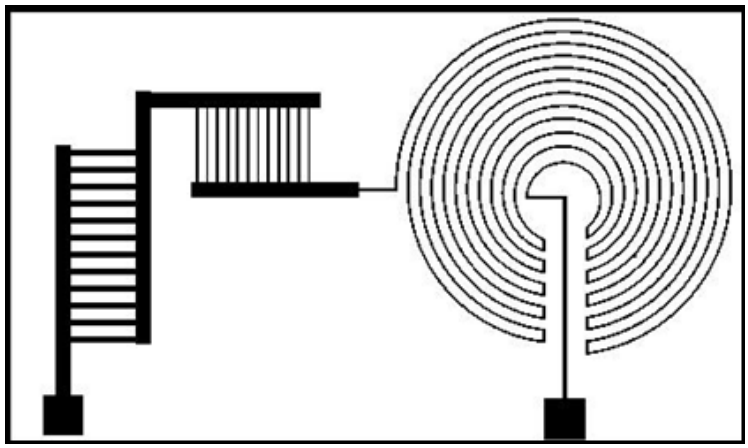

Figure 2-7: RF Design

2.4.2 Fabrication

To create a controllable gap between two electrodes for plasma generation, Figure 2-8 shows processes flow for the device. The initial steps are similar to the previous section's Part B (top electrode). After the mold was created, the following are process steps.

1. **Electroplating:** The resist formed acted as a mold. The gold slide was connected to the cathode and a platinum wire was anode. The current density was 15mA. The electroplating was performed for 15mins. The deposition rate was 0.4μm/min. 8μm of gold was deposited.
2. **Etch Process:** the resist on slides was removed with SU 8 resist stripper. The gold on slides was then etched with Gold etchant. A thin chrome seed layer present (J.T. Baker company) was etched by Chrome etchant.
3. **Clean:** The slides were cleaned with acetone followed by IPA and de-ionized water (DIW).

4. **Seal:** The slides were sealed with a glass slide with double sided tape. The sealing glass had two 1mm diameter holes drilled for gas inlet/outlet.

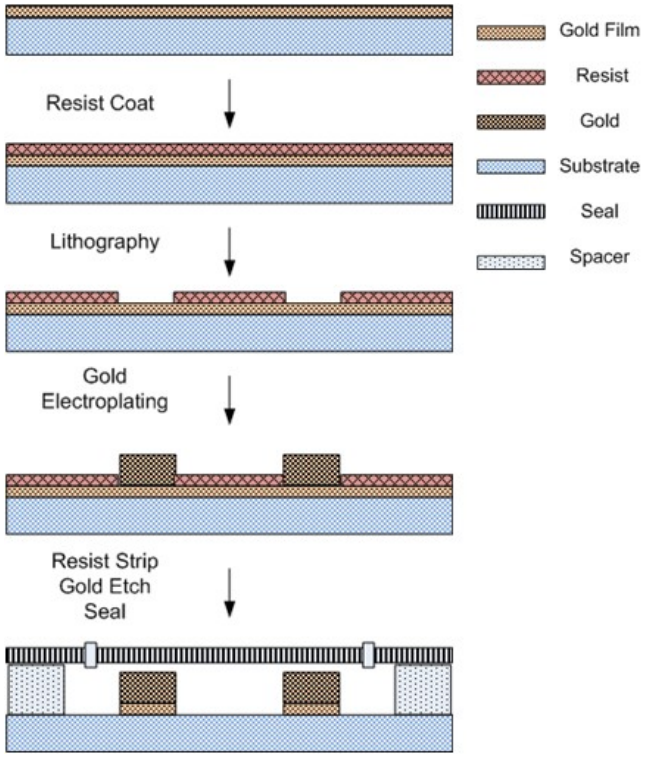

Figure 2-8: Processing Steps for RF Design, Electroplating Setup

Figure 2-9 shows the image after electroplating and the final device after etching.

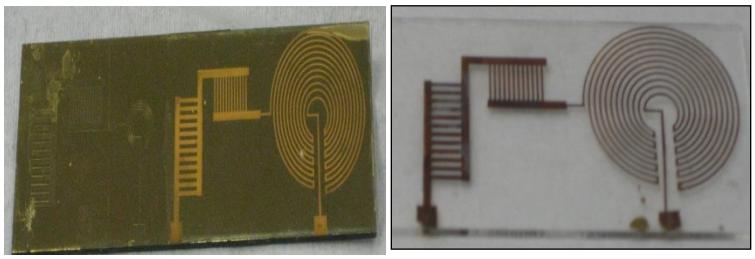

Figure 2-9: Gold Electroplating and Final Device

Chapter 3 - Characterization of Microplasma MEMS Device

In this chapter, the plasma characteristics under different conditions are explained. The fabricated devices are first characterized by I-V curves, followed by OES to determine the gas molecules and finally the testing of gases disassociated from plasma for energy generation in a PEM fuel cell. I-V characteristics for plasma with different carrier gases are presented. The effect of flow rate on plasma is discussed. OES data for Argon and Helium plasma are presented for devices. The OES is collected for carrier gas and for a mixture of water vapor and carrier gas plasma. A comparison is made between the two gases as a plasma source. The basic plasma characteristics are explained in Section 1.5.

3.1 DC Setup for I-V Characterization

The primary aspect of the project was to generate micro scale plasma at atmospheric pressure and low voltage. The easiest method of determining plasma was by its I-V characteristics. The set up, as in Figure 3-1, was used. A DC power supply (Kepco) was used. The negative output was connected to one of the two electrodes of plasma device. The positive output was connected to 2 MΩ Resistor; this was connected in series to a multimeter for current measurement. The output from the meter was connected to the second electrode. The supply voltage was measured along with the circuit current. Negating the voltage of resistor from the supply voltage gave the plasma voltage. From here the plasma I-V curve was characterized.

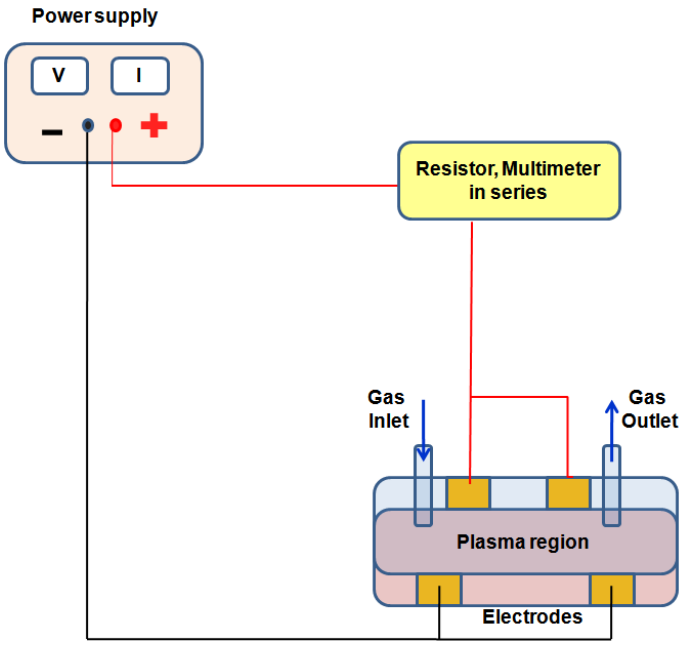

Figure 3-1: Schematic DC Test Setup

3.2 Optical Emission Spectroscopy and Hydrogen Generation Set Up

The second aspect of the project was to generate hydrogen from the microplasma. For achieving this, Ar/He gas was bubbled through water in a container. The output was a mixture of water vapor and the inert gas being used. This mixture was flown through the plasmas device and plasma was generated. The plasma generated with and without vapor was measured for intensity peaks using OES meter. The OES meter plotted wavelength (nm) vs. intensity (counts). The peaks were determined based on the constituent particles present in the gas. When water vapor was present, H, O peaks was visible. In the absence of water vapor, these peaks were absent.

The setup for this process is shown in Figure 3-2 below. The relative humidity was measured. From this absolute, humidity was found with the amount of water present in flowing gas determined. The Appendix includes related data.

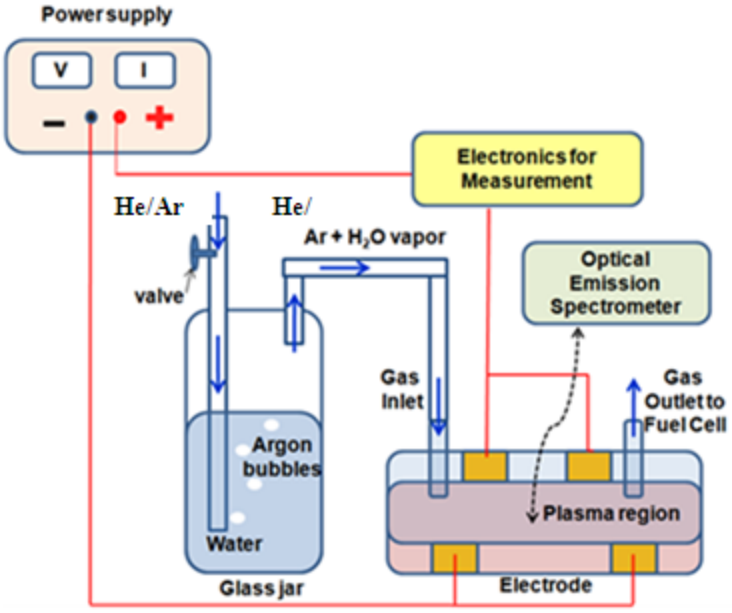

Figure 3-2: Schematic of Setup for Hydrogen Generation

3.2.1 OES

Ocean Optics HR4000 Spectrometer was used to collect spectra. There are several parts in the meter, including (1) Subminiature version A (SMA) connector, (2) Slit, (3) Filter, (4) Collimating mirror, (5) Grating, (6) Focusing mirror, (7) Collection lens, and (8) Charge-coupled device (CCD) detector.

The emissions enter from connector (1). The emissions are then split and separated based on emission wavelengths with the help of slit, filter and other components of OES. The split emissions are collected with the help of a CCD. This spectra collected determines the material present in light source; in our case, this source is microplasma.

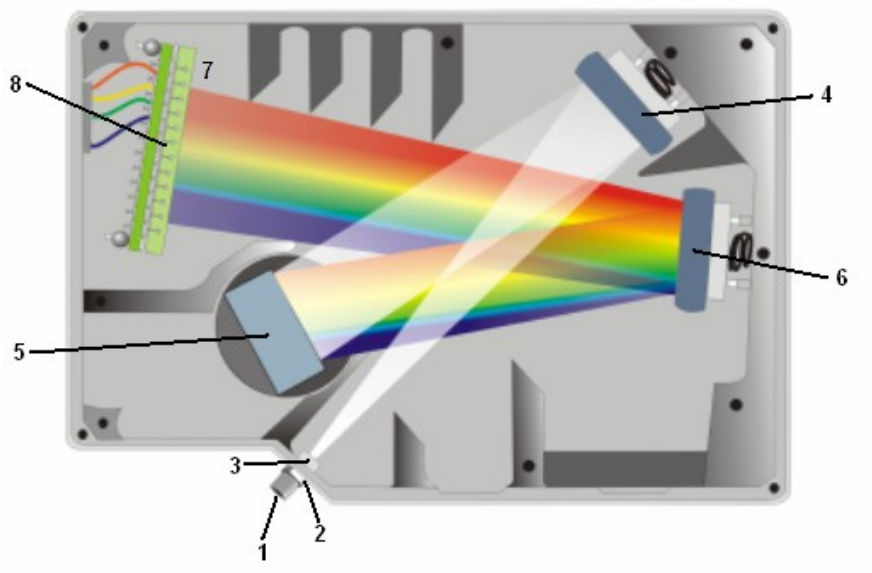

Figure 3-3: OES Spectrometer Schematic [20]

Each material has its own specific spectral lines. The spectral lines for each individual elemant is catalogued on the NIST spectral line webpage [21]. The gases of interest for our experiment are hydrogen and the carrier gases used. These lines are identified and looked for in the OES data collected to determine the atoms presemt in plasma. Figure 3-4 shows the OES output for plasma device. The range for which data is collected is from 200nm to 1200nm. The range useful to us is between 400-700nm, with the wavelengths being where hydrogen spectra are visible. For this reason the other wavelengths are not plotted for analysis. The peaks are dependent on the carrier gas and the gas mixture.

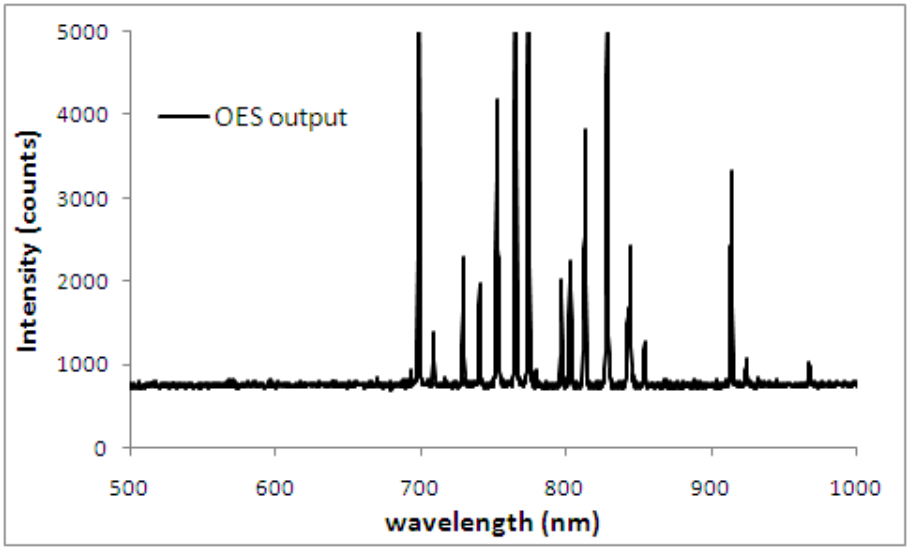

Figure 3-4: OES Output

Figure 3-5 shows the peaks for Argon and Helium plasma. These peaks were present in all the OES data collected. These peaks are not shown in the OES analysis as explained earlier.

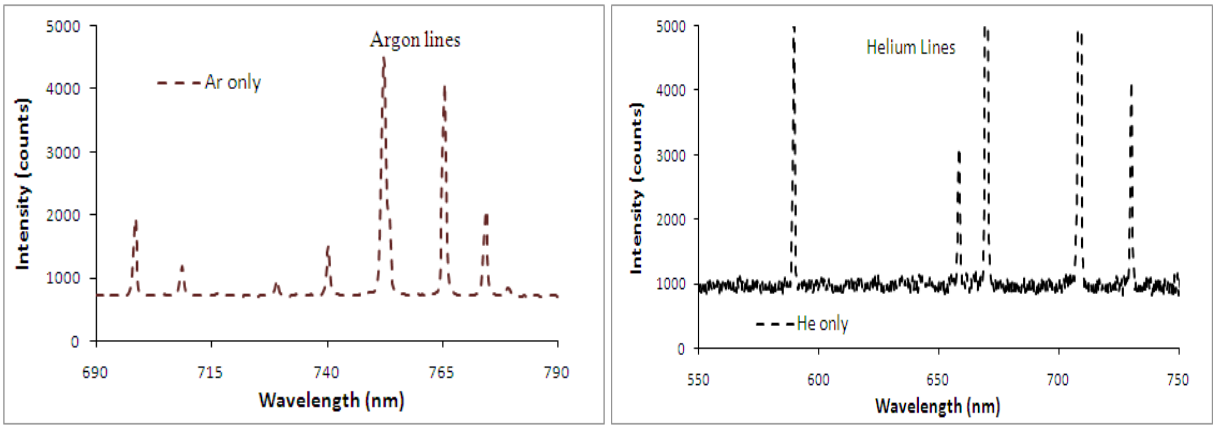

Figure 3-5: OES Peaks for Argn and Helium

3.3 Fuel Cell Voltage Test Setup

The final aspect of the project was to use the hydrogen generated for generating voltage in a PEM fuel cell. The OES data of plasma showed that hydrogen atoms were present for both coplanar and parallel plate devices. Hydrogen was also present with both carrier gases (Argon & Helium). The Fuel cell test was done with only coplanar device. The reason being the life time of ITO electrode was limited to around 15 minutes. The electrodes designed were such that plasma was genrated in a small regions. In the case of a coplanar device, the life time was more than one hour. The electrode design allowed long plasma regions. It was assumed that the more plasma generated, the more hydrogen generated. The setup for testing Hydrogen with Fuel cell was as shown in the Figure 3-6. The oxygen was supplied from the elctrolysis process. This was stored in the oxygen chamber. The hydrogen from electroplating was drained from the storage chamber and substituted with the gas mixture from plasma chamber. The mixture of carrier gas, water vapor was flown into the hydrogen part cell of the Fuel cell, after passing over plasma region.

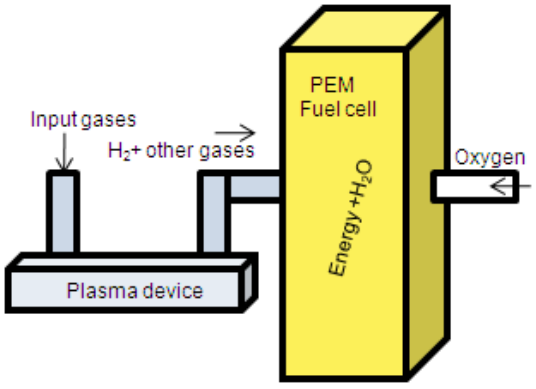

Figure 3-6: Fuel Cell Test Setup

Figure 3-7 shows the image of setup for Fuel cell test setup. As seen Helium/Argon gas can be switched as required. For fuel cell setup the outlet from flow meter goes into the bubbler. The output of bubbler is connected to the input of plasma device. The output from plasma device is inserted into the hydrogen storage chamber of fuel cell. The hydrogen cell seal was left open to allow continuous flow of input gases.

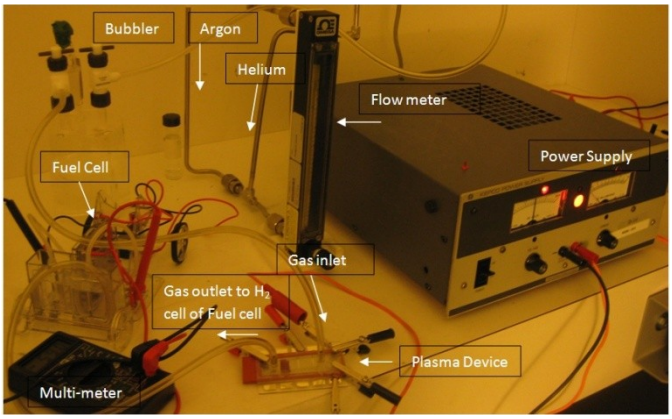

Figure 3-7: Image of Test Setup

Figure 3-8 shows the I-V plot for parallel plate device with Argon and Helium carrier gas. The sustenance voltage for Helium plasma is much less than Argon plasma. For Argon plasma, the sustenance voltage is 210V in case of Helium of plasma it was around 155V.

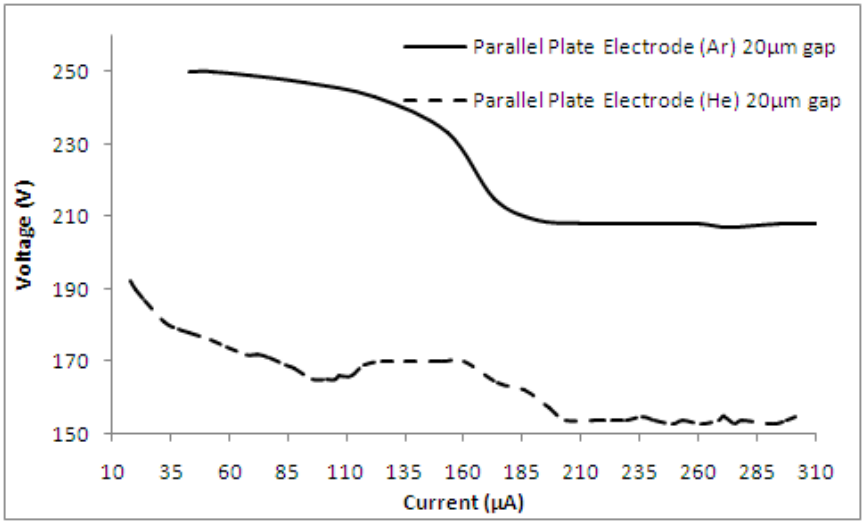

Figure 3-8: I-V Plot for Parallel Plate Device with Argon & Helium

3.4 OES Data

Figure 3-9 shows the OES data from plasma with Argon only as well as with water vapor and Argon for parallel plate electrode design. Hydrogen peaks are visible at 486nm and 656nm. This shows plasma-disassociated water vapor. The oxygen peaks indicate dissociation of ITO electrode

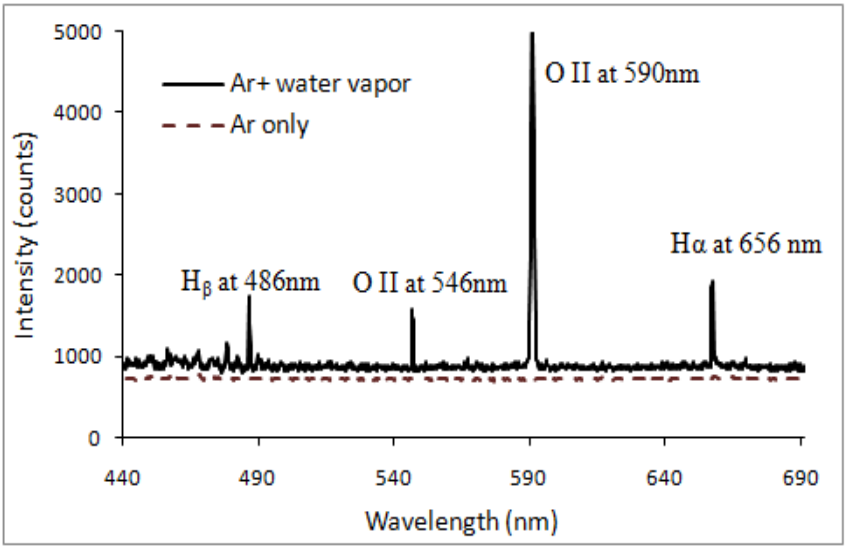

Figure 3-9: Spectra of Argon Plasma for Parallel Plate Device

In Figure 3-10, the OES data from plasma with Helium only as well as with water vapor and Helium for parallel plate electrode device are shown. Hydrogen peaks are visible at 486nm and 656nm. This shows plasma-disassociated water vapor. The oxygen peaks indicate dissociation of ITO electrode. In case of helium plasma, peak is observed at 587 for both coplanar and parallel plate device. This is the peal of Helium. When water vapor is introduced into parallel plate device, the oxygen and helium peaks are indistinguishable.

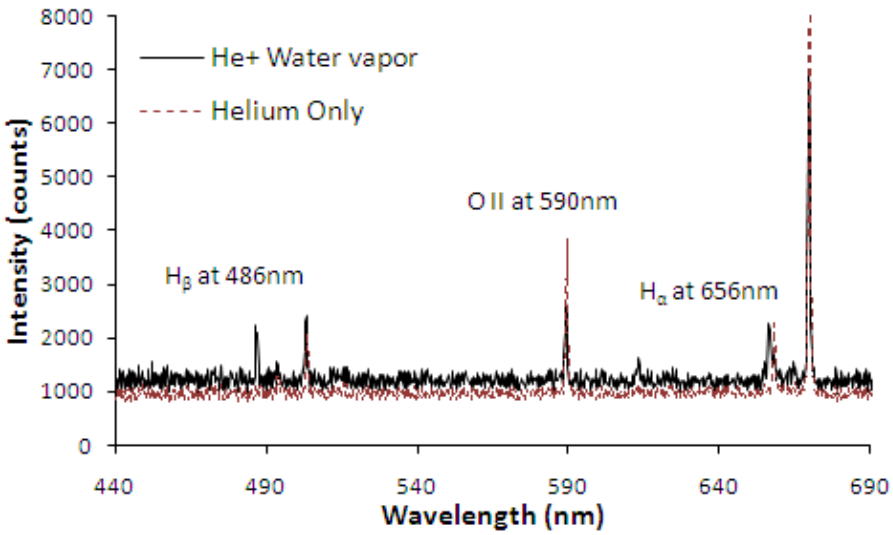

Figure 3-10: Spectra of Helium Plasma for Parallel Plate Device

Figure 3-11 depicts the I-V plot for coplanar device with Argon and Helium carrier gas. The sustenance voltage for Helium plasma is much less than Argon plasma. For Argon plasma, the sustenance voltage was 230V in case of Helium of plasma it was around 165V.

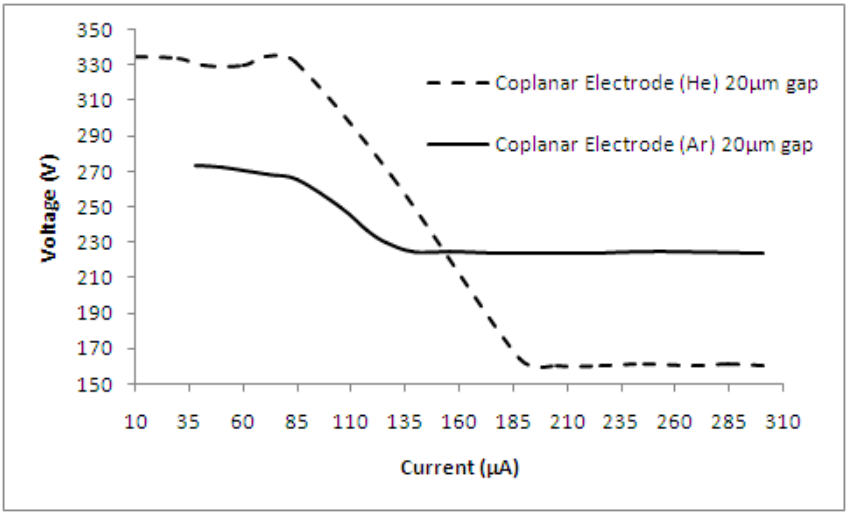

Figure 3-11: I-V Plot for Coplanar Device with Argon & Helium

Figure 3-12 shows the OES data from plasma with Argon only and with water vapor and Argon for coplanar device. Hydrogen peaks are visible at 486nm and 656nm. This shows plasma-disassociated water vapor.

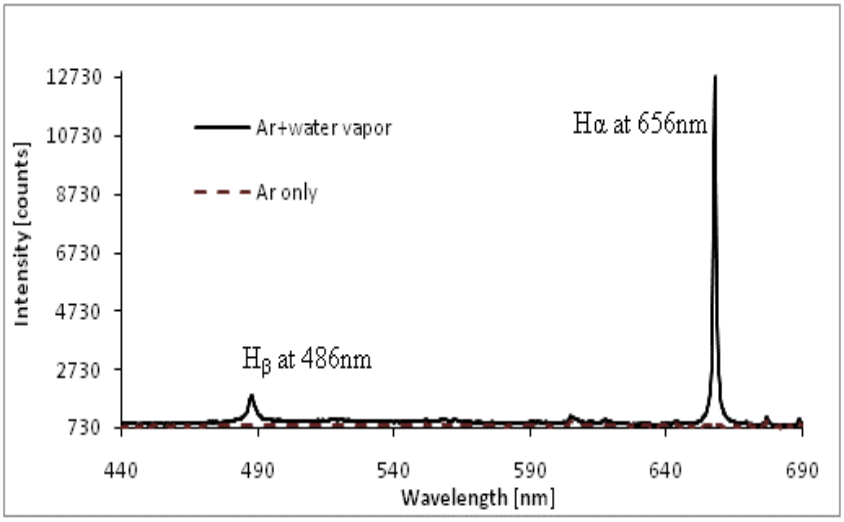

Figure 3-12: Spectra of Argon Plasma for Coplanar Device

Figure 3-13 shows the OES data from plasma with Argon only as well as with water vapor and Argon for coplanar device. Hydrogen peaks are visible at 486nm and 656nm. This shows plasma-disassociated water vapor.

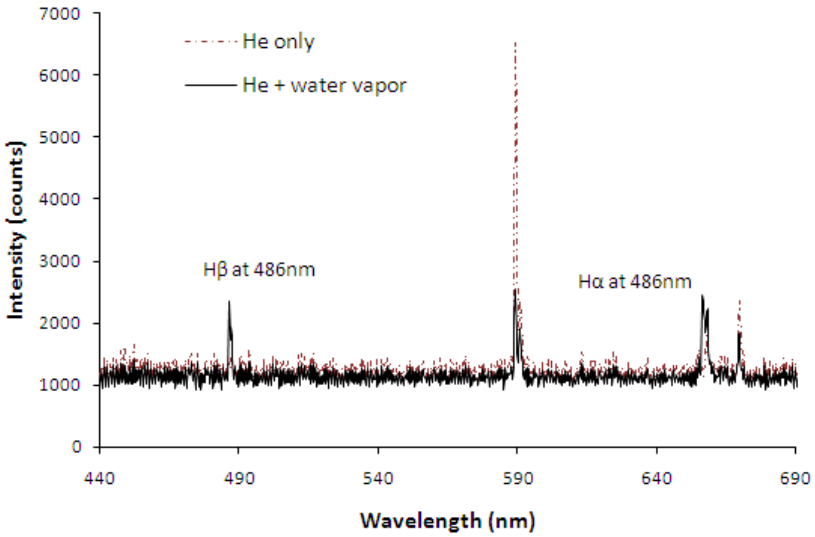

Figure 3-13: Spectra of Helium Plasma for Coplanar Device

3.5 Fuel Cell Analysis

Figure 3-14 shows fuel cell voltage being generated with a constant plasma voltage with Argon carrier gas. The initial fuel cell voltage starts from 23mV when Argon and water vapor mixture flow into fuel cell. This could be some kind of leakage error. The fuel cell takes approximately 35minutes to reach the maximum voltage of 43mV. The gas flow is maintained at 55sccm.

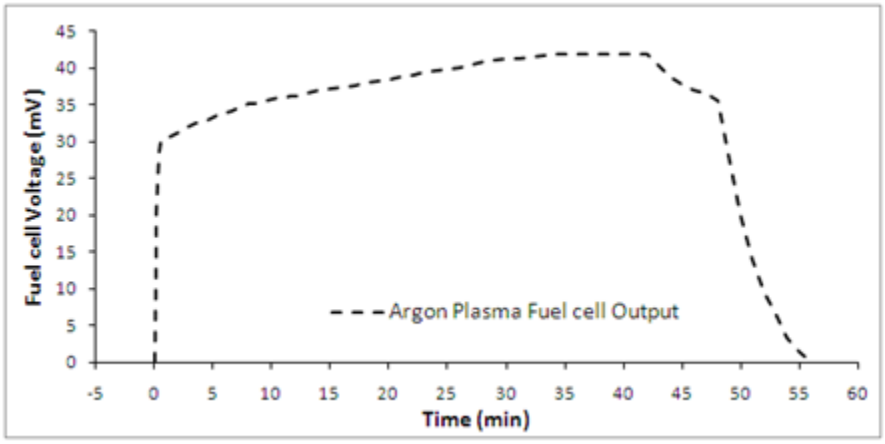

Figure 3-14: Fuel Cell Voltage Test for Coplanar Device with Argon

Figure 3-15 shows fuel cell voltage being generated with a constant plasma voltage with Helium carrier gas. There was no initial voltage as from previous case. The gas mixture generated a maximum of 61.7mV. This is nearly three times higher than the results from Argon plasma.

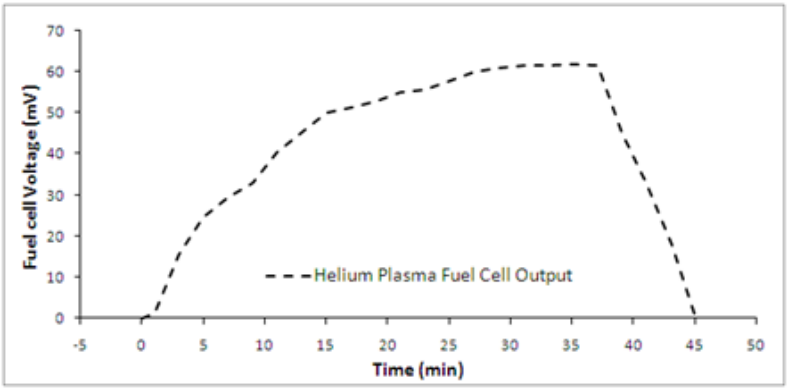

Figure 3-15: Fuel Cell Voltage Test for Coplanar Device with Helium

Figure 3-16 shows fuel cell voltage being generated with a constant plasma voltage with Argon carrier gas followed by Helium gas. After the voltage generated from Argon plasma stabilized, the Argon gas was shut off and Helium gas was turned on. Argon plasma generated a maximum voltage of 21.6mV. This is the same as in first case without the addition of initial voltage from fuel cell. This plot shows the maximum voltage Argon gas plasma generated is three times less than Helium plasma with the other conditions being similar.

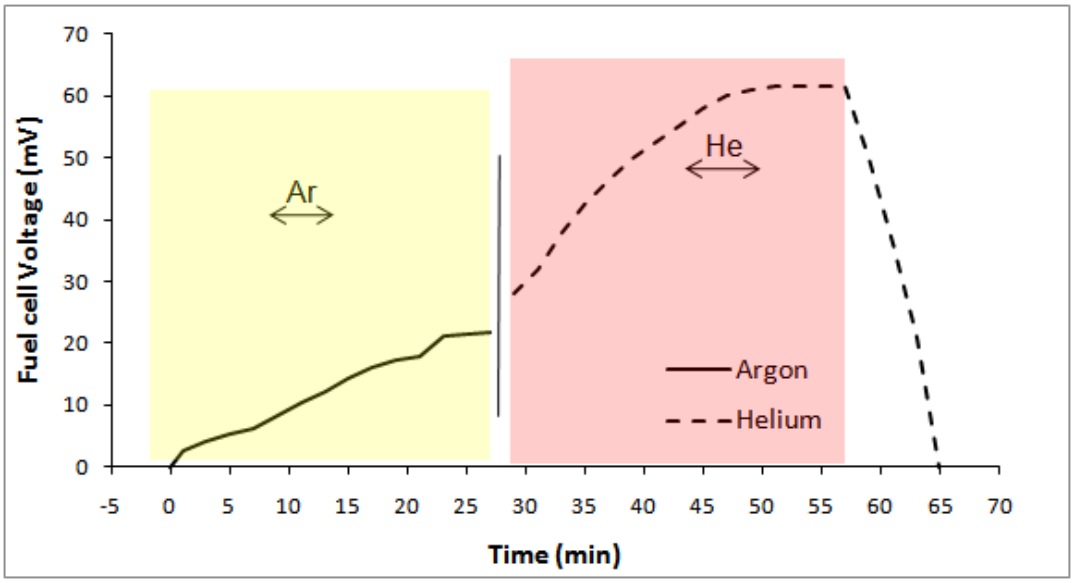

Figure 3-16: Fuel Cell Voltage Test for Coplanar Device with Argon & Helium

For generating hydrogen and oxygen from fuel cell a bulb can be used as substitute for sunlight. A normal glow light (fluorescent) though can generate voltage from Solar cell; this voltage is not enough for splitting water. When hydrogen from the storage chamber is drained (oxygen present) the fuel cell voltage goes to zero. Similarly when oxygen is drained (hydrogen present) from the chamber the fuel cell voltage doesn't go to zero. The fuel cell generates about 100mV. When the gas mixture from plasma device is sent into the oxygen chamber of fuel cell; it generates some voltage. This could be because of the oxygen present in the mixture.

Figures 3-17 and 3-18 show the plasma glow at different flow rates for Argon and Helium gases for parallel plate device. In case of Argon at 40sccm the plasma glow was weak, at 70 sccm the glow was brightest and at 100 sccm the glow was flickering. This was evident from the plasma voltage as shown in the above table. The plasma voltage fluctuated considerably. The other test conditions were not changed. The supply voltage was set to 500 V. The circuit current changed as the flow rate was changed. In case of Helium at 40 sccm the glow was bright in comparison to Argon gas and the plasma got brighter at as the flow rate was increased. There was no flickering observed at 100sccm. The circuit current was almost constant at different flow rates.

The current-voltage table shows that voltage and current changed minimally for Helium gas while the fluctuations were much greater for Argon gas. The sustenance voltage for Helium gas reduced from Argon gas.

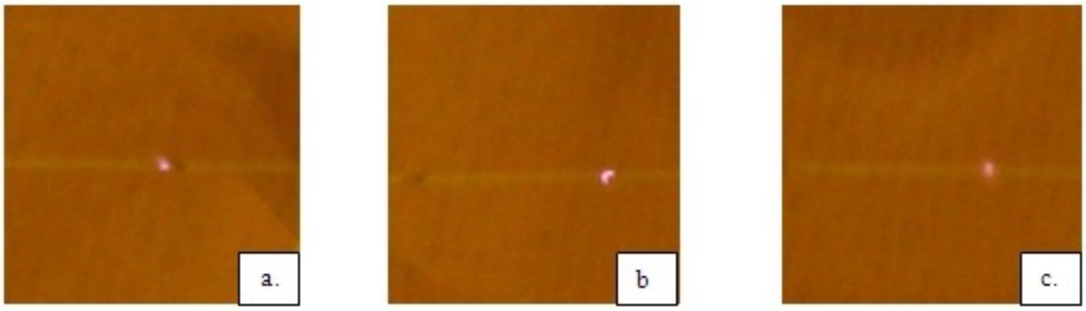

Figure 3-17: Argon Flow at 40, 70, 100 sccm Respectively for Parallel Plate Device

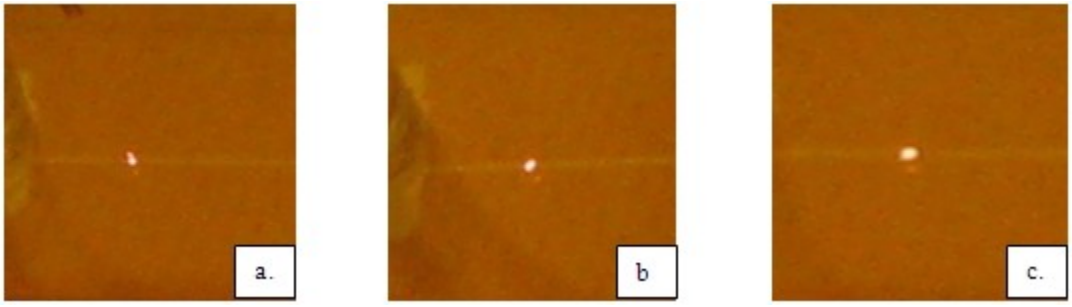

Figure 3-18: Helium 40, 70, 100 sccm Respectively for Parallel Plate Device

Device	Carrier gas	Flow rate	40sccm	70sccm	100sccm
Parallel Plate	Argon	**I(μA)**	150	145	135
ITO		**V(V)**	200	210	230
Parallel Plate	Helium	**I(μA)**	166	163	159
ITO		**V(V)**	168	174	182

Table 3-1: I-V Data at Different Flow Rates for Parallel Plate Device

Figures 3-19 and 3-20 show the plasma glow at different flow rates for Argon and Helium gases. As in the case of parallel plate device the results for coplanar device were similar. In case of Argon at 40sccm, the plasma glow was weak. At 70 sccm, the glow was brightest. At 100sccm, the glow was flickering. This was evident from the plasma voltage as shown in the table above. The plasma voltage fluctuated considerably. The other test conditions were not changed. The supply voltage was set to 500V for Helium flow while the supply voltage was changed to 540V and 560V for 70sccm & 100sccm for Argon plasma measurements. The circuit current changed as the flow rate was changed. In case of Helium at 40sccm was bright in comparison to Argon gas and the plasma got brighter at as the flow rate was increased. The circuit current was almost constant at different flow rates.

The I-V table shows the changes for helium plasma were not significant. In case of Argon plasma the supply voltage had to be increased for sustaining the voltage.

This experiment showed that Helium is better for plasma generation at different flow rates. The voltage didn't fluctuate as in the case of Argon gas.

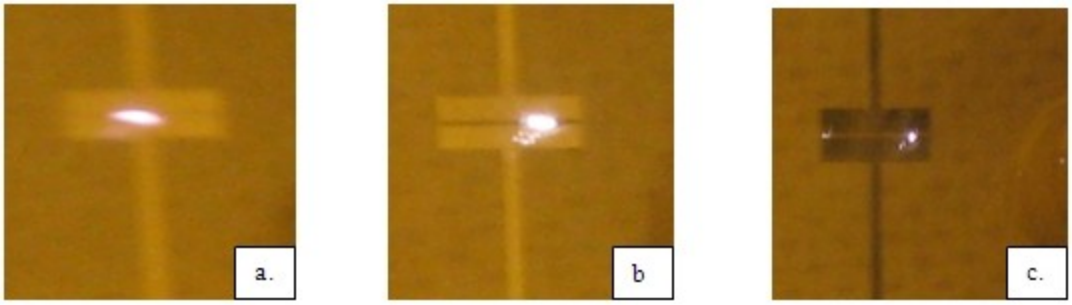

Figure 3-19: Argon Flow at 40, 70 and 100sccm for Coplanar Device

Figure 3-20: Helium Flow at 40, 70 and 100sccm for Coplanar Device

Device	Carrier gas	Flow rate	40sccm	70sccm	100sccm
Coplanar	Argon	I(μA)	130	160	170
Aluminum		V(V)	240	220	230
Coplanar	Helium	I(μA)	167	169	166
Aluminum		V(V)	166	162	168

Table 3-2: I-V Data at Different Flow Rates for Coplanar Device

Figure 3-21 shows plasma for Argon and Helium with a parallel plate device. Argon-sustained plasma at 230V and helium at 165V. The flow rate and gap were 55sccm and 20 μm, respectively.

Figure 3-21: Plasma with Argon and Helium Gas in Parallel Plate Device

The Figure 3-22 shows plasma for argon and helium plasma coplanar device. Argon sustained plasma at 370V (gap 500µm) and Helium at 170V (gap 20µm). The flow rate and gap was 55sccm

Figure 3-22: Plasma with Argon and Helium Gas in Coplanar Device

Chapter 4 - RF Design and Results

The DC plasma results were encouraging. One main drawback of DC plasma was the lifetime of electrodes (aluminum and ITO) was short. This was because of the electron bombardment of electrodes. A RF supply was much less stressful on the electrodes. To characterize RF plasma, the devices were tested with a 13.56MHz supply.

Figure 4-1 shows the setup for microplasma generation and characterization with a RF supply (13.56MHz). The power supply is specially designed for this purpose. The power supply has output in Watts, with the power forward and power reflected being approximately 10% for obtaining the best results. The RF power supply consists of two modules; namely, the power supply and the matching network. The RF supply has an indicator lamp, which illuminates as the capacitance of the circuit increases. Ideally, this light should not illuminate. The output cable has two connectors. One is the signal wire and the other is ground. The signal wire has the entire signal and must be handled with caution. The capacitance for the devices should be less than 50pF.

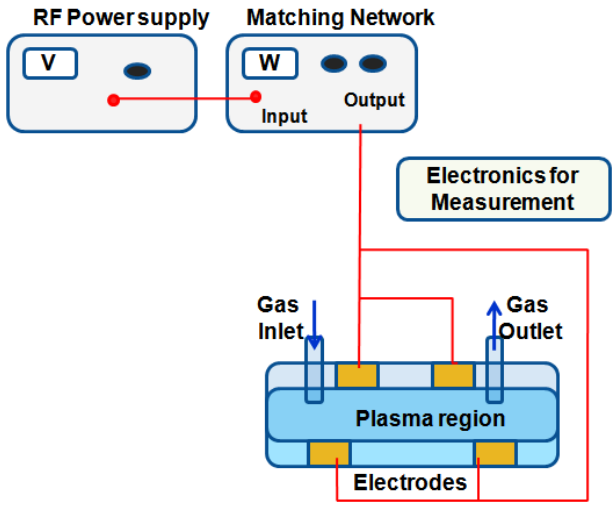

Figure 4-1: RF Device Test Setup

4.1 First Attempt: Coplanar and Parallel-Plate Electrode Devices for RF Microplasma

The coplanar and parallel plate devices fabricated for DC testing were used for the first attempt of generating RF plasma. The coplanar and parallel plate devices were connected to signal and ground of RF power and tested for plasma. In case of coplanar device, there was plasma at 8W. The plasma was very bright and hot (evident from substrate cracking). This lead to very rapid disintegration (3 mins) of the electrode and caused the glass substrate to crack.

In case of parallel plate device, the resist which acted as seal and gap melted and the substrate cracked. The resist melted when the power supplied was 5W. This lead carrier gas to escape and no plasma was generated.

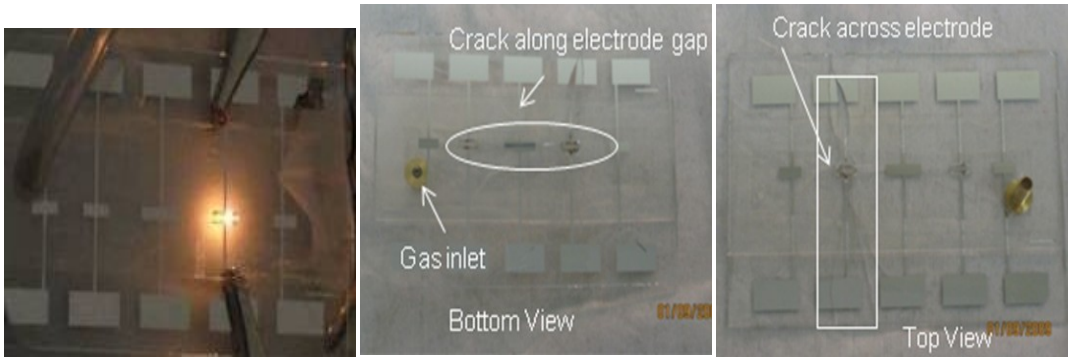

Figure 4-2: RF Plasma & After Effects

4.2 The Second Attempt: Coil Design

4.2.1 Device Design

The device design was adapted from a paper authored by Dr. J. Hopwood of Northeastern University titled "A microfabricated inductively charged plasma generator"[19]. In this paper they showed the following results

- The plasma is sustained without electrodes by inductively coupling a 450 MHz current into a region of low pressure gas.

- Both argon and air plasmas are generated over a range of gas pressures from 0.1 torr to 10 torr (13.3 Pa - 1333 Pa).
- The power used to sustain the plasma is 350 mW, although ~1.5 W is required to initiate the discharge.
- Network analysis of the plasma generator circuit shows over 99% of the applied RF power can be absorbed by the device. Of this, ~50% is absorbed by the plasma and the remainder of the power is dissipated as ohmic heating.
- An argon ion current of up to 4.5 mA/cm^2 has been extracted from the plasma and the electron temperature is 52,000 K at 0.1 torr.

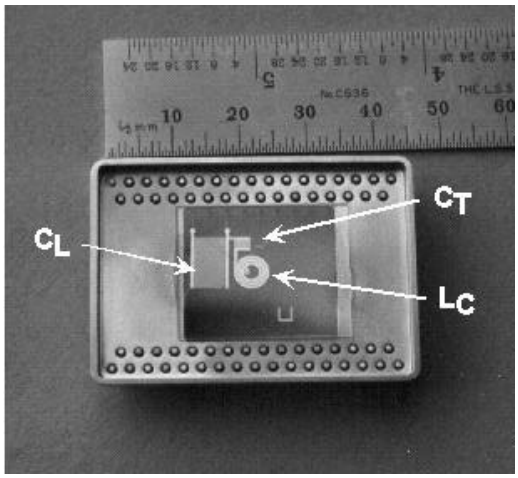

Figure 4-3: RF Plasma Device [19]

The results were similar to our goals of low power plasma; hence, the design was used.

4.2.2 Fabrication

The fabrication steps were explained in Section 2.4.2. The initial steps were similar and repetitive. A new process flow for electroplating was designed. Gold electroplating process was developed. The process development required selection of the best resist and determination of the current density for even deposition. The electrolyte contained potassium cyanide. Therefore, work was performed with extreme caution.

Figure 4-4 shows electroplating setup for electroplating gold. The anode is a platinum wire; cathode is the gold substrate with Su 8 resist mold. The electrolyte solution contains gold particles; cations are formed when a current is passed through the setup. The solution is at 60 ^{0}C. The gold deposition rate is determined by the current flown. Lower flow ensures even deposition. The current density is set at 15mA and the deposition rate is 0.4µm/min.

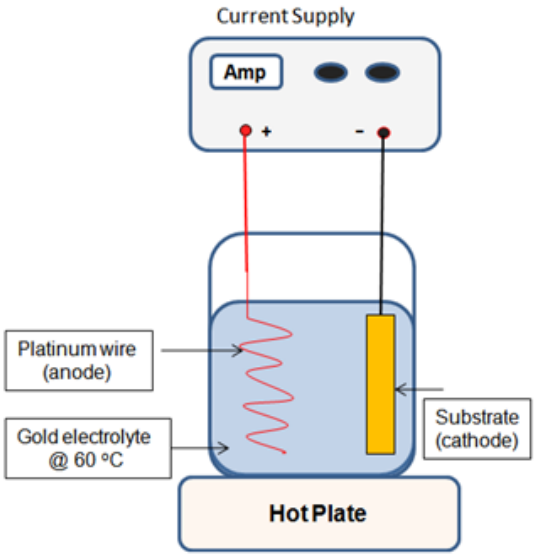

Figure 4-4: Gold Electroplating

4.3 Process Development

Figure 4-5 a) is a mold with AZ9260 while Figure 4-5 b) is electroplating on gold substrate with AZ mold. The figure shows the electroplating process flow development. A mold is made with AZ9260 resist on gold substrate with electroplating performed on this mold. The electroplating process is performed. The resist peels off. The resist peels off in the solution and with deposition all over the substrate. While the resist has a good mold, it is not strong enough for the electroplating process. AZ9260 is discarded.

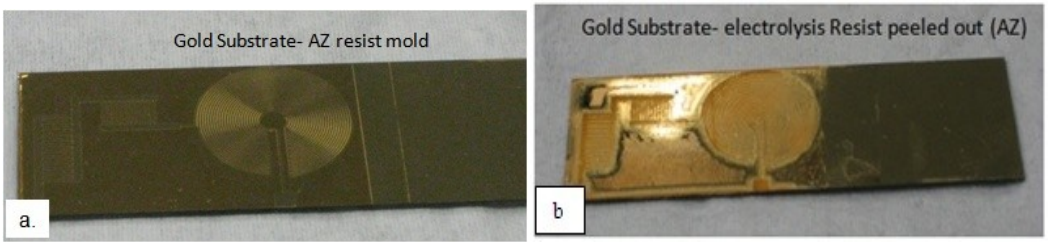

Figure 4-5: Process Development

The same process as before was followed for SU 8 resist. First the mold was made followed by electroplating. Figure 4-6 shows the electroplated substrate. The SU 8 mold was strong and the deposition was uniform. SU 8 resist was used for processing.

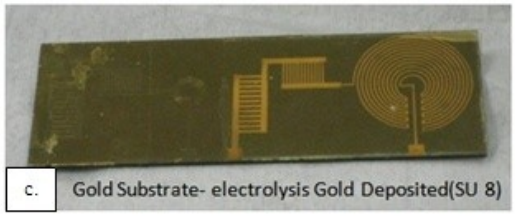

Figure 4-6: c) Electroplating on Gold Substrate with SU 8 Mold

SU 8 resist was chosen as mold and the processing was done. The first step (a) being creating a mold on the slides, followed by (b) electroplating, and finally (c) resist stripping, gold and chrome seed layer etching, the process images are shown in Figure 4-7.

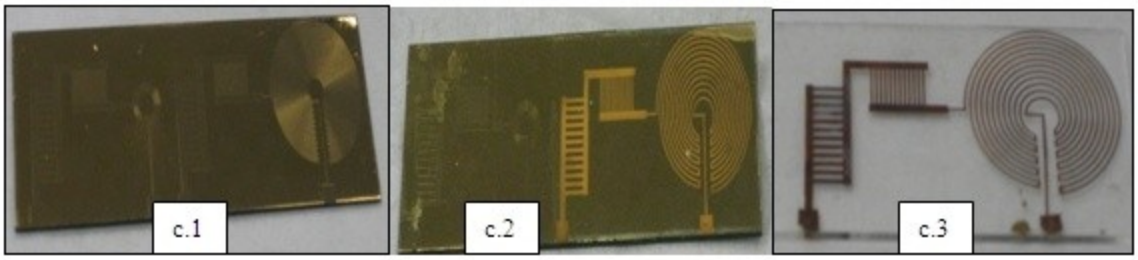

Figure 4-7: RF Device

The coil design had same overheating issue as the coplanar and parallel plate designs. The glass substrate cracked when RF power was applied. The power at which it cracked was 8W. The power was increased to the previous maximum voltage in a couple of minutes. There was no plasma, but the substrate cracked.

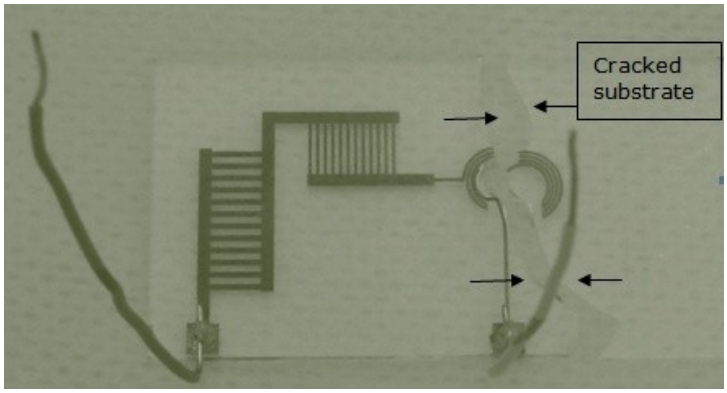

Figure 4-8: RF Device After Testing

A new process flow for the RF device, which does not generate heat, has to be designed. In the coil design, no plasma was generated. The devices cracked before any plasma was generated. The design on which this device was based was tested in a low-pressure environment, with variable output frequency and power. This could be a reason why the coil device was not functional. A power supply, which has more options than the one present, could help solve the issue.

Chapter 5 - Conclusion and Future Work

5.1 Conclusion

The project showed that Plasma can be generated at low DC voltage and at atmospheric pressure. Argon and Helium gases generated plasma. Plasma with Argon was at slightly higher voltages than at Helium. This was most likely because Argon was much heavier and larger than Helium, though Argon requires lesser energy (15.5ev/atom) for exciting electrons than helium (24.8ev/atom). Coplanar and parallel plate devices for the same electrode gap had identical, but not exactly the same results. Parallel plate device had lower ignition and sustenance voltage than coplanar device for both Argon and Helium. ITO lifetime was limited. Few hundred nanometers of Magnesium Oxide (MgO) film was deposited on ITO electrodes. This did not help in improving the lifetime. The Aluminum electrode life time depended on the thickness of film. The thicker the film, the longer was the life time. 1.2μm aluminum film has a lifetime of longer than 1 hour. ITO film was much stronger in comparison. ITO film was 750 Angstrom thick and had a life time of approximately 15minutes. The fuel cell used was from Thames and Kronos Fuel Cell Car Kit. The voltage generated from recombination of Hydrogen and Oxygen was 0.9V. Argon plasma generated much less voltage than Helium plasma from the fuel cell. The maximum voltage from Argon plasma in the fuel cell was 21.7mV and in case of helium plasma it was 61.7mV.

The fabrication process for devices is simple and repeatable. All the devices can be fabricated in any lab where the tools are available. All the materials used are commonly used in semiconductor processing. Fabrication process of either coplanar, parallel plate or RF device is less than a day's work.

I-V characteristics of devices showed that plasma can be generated and sustained at lower voltage for Helium than Argon. Helium plasma is more consistent at varied gas flow rates. Based on Paschen curves the I-V characteristics of Argon and Helium should be similar for the given p*d. This was not the case. The reason could be the atomic size of the gases.

RF device testing was not successful. The plasma generated was thermal in nature and caused substrate to crack and rapid degradation of electrode. Plasma was generated at 8W power with the coplanar device. A thick electrode is supposed to reduce heat being generated. This did not happen. In the new coil design, electrodes were 7µm thick. A new substrate is to be found or the design changed.

5.2 Future Work

The electrode life time has to be improved considerably. This can be achieved by increasing the thickness of the electrode. An insulating material on top of the electrodes reduces the electrode disintegration.

A method for separating hydrogen from mixture of gases is to be looked into for improving the efficiency of plasma device. Most of the hydrogen separation techniques available are energy consuming techniques, which require high temperature and/or high pressure. A cost-efficient method of separation of gases will make microplasma device very efficient.

References

[1] F. Joensen and J. R. Rostrup-Nielsen, "Conversion of hydrocarbons and alcohols for fuel cells," *Journal of Power Sources,* vol. 105, pp. 195-201, Mar 20, 2002.

[2] R. M. Navarro, M. A. Pena, and J. L. G. Fierro, "Hydrogen production reactions from carbon feedstocks: Fossils fuels and biomass," *Chemical Reviews,* vol. 107, pp. 3952-3991, Oct 2007.

[3] F. Joensen, J.R. Reostrup-Neilsen, Journal of Power Sources 105 (2002) 195–201.

[4] J. Turner, G. Sverdrup, M.K. Mann, P.-C. Maness, B. Kroposki, M. Ghirardi, R.J. Evans, D. Blake, International Journal of Hydrogen Energy 32 (2008) 379–407.

[5] J.M. Norbeck, J.W. Heffel, T.D. Durbin, B. Tabbara, J.M. Bowden, M.C. Montani, Hydrogen Fuel for Surface Transportation, Society of Automotive Engineers Inc., Warrendale, PA, 1996, p. 548.

[6] J. Turner, G. Sverdrup, M.K. Mann, P.-C. Maness, B. Kroposki, M. Ghirardi, R.J. Evans, D. Blake, International Journal of Hydrogen Energy 32 (2008) 379–407.

[7] Solar Photoproduction of Hydrogen by James R. Bolton, Department of Chemistry, The University of Western Ontario.

[8] J. Akikusa, S.U.M. Khan, International Journal of Hydrogen Energy 27 (2002) 863–870.

[9] Catastrophes, Chaos & Convolutions, Baen Books http://www.jamesphogan.com/bb/CPG.

[10] Peratt, A.L., "Advances in Numerical Modeling of Astrophysical and Space Plasmas," (1966) Astrophysics and Space Science, v. 242, Issue 1/2, p. 93-163.

[11] Y. P. Raizer, Gas Discharge Physics: Springer-Verlag, 1987.

[12] D. Mariotti, J. A. McLaughlin, and P. Maguire, "Experimental study of breakdown voltage and effective secondary electron emission coefficient for a micro-plasma device," *Plasma Sources Science & Technology,* vol. 13, pp. 207-212, 2004.

[13] http://www.scielo.br/img/revistas/bjp/v34n4b/a15fig02.gif (last visited August 14, 2009).

[14] K. Tachibana, "Basic aspects of microplasmas and their future prospects," Oyo Buturi, Vol. 75, pp. 399-411, 2006 [in Japanese].

[15] Schoenbach K.H., El-Habachi A., Shi W., Ciocca M. *Plasma Sources Science Technology* 1997; **6**:468.

[16] Stark R.H., Schoenbach K.H.. *Journal of Applied Physics* 1999; **85**:2075.

[17] Sakai O., Kishimoto Y., Tachibana K., *Journal of Physics D: Applied Physics* 2005; **38**:431.

[18] Ito T., Terashima K., *Applied Physics Letters* 2002; **80**:2648

[19] Iza F., Hopwood J., *Plasma Sources Science Technology* 2005; **14**:397.

[20] O. I. F. i. Photonics, "QE65000 Scientific-grade Spectrometer, Installation and Operation Manual," 2007.

[21] Z. Yan, L. Chen, H. Wang, Xuebao Huagong/Journal of Chemical Industry and Engineering (China) 57 (2006) 1432–1437.

[22] A. Czernichowski, P. Czernichowski, K. Wesolowska, Fuel Cell Science, Engineering and Technology—2004, Plasma-Catalytical Partial Oxidation of Various Carbonaceous Feeds into Synthesis Gas, American Society of Mechanical Engineers, New York, United States/Rochester, NY, United States, 2004, pp. 669–676.

[23] H. Sekiguchi, Y. Mori, Thin Solid Films, Steam Plasma Reforming Using Microwave Discharge, Elsevier, Jeju Island, South Korea, 2003, pp. 44–48.

[24] R.B. Biniwale, A. Mizuno, M. Ichikawa, Applied Catalysis A: General 276 (2004) 169–177.

[25] C.J. O'Brien, S. Hochgreb, A. Rabinovich, L. Bromberg, D.R. Cohn, in: Proceedings of the Intersociety Energy Conversion Engineering Conference, Hydrogen Production via Plasma Reformers, IEEE, Piscataway, NJ, USA/Washington, DC, USA, 1996, pp. 1747–1752.

[26] T. Paulmier, L. Fulcheri, Chemical Engineering Journal 106 (2005) 59–71

[27] L. Bromberg, D.R. Cohn, A. Rabinovich, N. Alexeev, International Journal of Hydrogen Energy 24 (1999) 1131–1137.

[28] Holladay JD, J Hu, DL King, and Y Wang. 2009. "An Overview of Hydrogen Production Technologies." Catalysis Today 130(4):244-260.

Appendix

S.no	process	process detail	Process time
1	Coat PR	Coat HPR-504 using standard prog (+ve resist). 1.2um	500RPM for 10sec thn 3000RPM for 60sec
2	Bake	Bake at 115 C	1 min 30 sec
2	Expose	Expose on Karl Suss MA 55	15sec
3	Develop	Develop the Resist in CD- 26	45 sec
4	Etch	Etch ITO in HCl, H20 bath (1:1)	1-2min
5	Strip	Strip resist in Acetone, clean with IPA	30 sec

S.no	Process	Process detail	Process time
1	Coat PR	Coat AZ 9260 positive resist (18.7um thickness)	500RPM for 10sec thn 750RPM for 60sec
2	Bake	AZ9260 PEB @ 115 degree celcius	2min
3	Expose	Expose on Karl Suss (approx 2100 mj/cm^2)	300sec
4	Develop	Develop the Resist in AZ400K (1:4) developer to water ratio	6 min

Figure A-1: Process Flow for Parallel Plate Device with AZ9260 Resist

S.no	process	process detail	Process time
1	Coat PR	Coat HPR-504 using standard prog (+ve resist). 1.2um	500RPM for 10sec thn 3000RPM for 60sec
2	Bake	Bake at 115 C	1 min 30 sec
2	Expose	Expose on Karl Suss MA 55	15sec
3	Develop	Develop the Resist in CD- 26	45 sec
4	Etch	Etch ITO in HCl, H20 bath (1:1)	1-2min
5	Strip	Strip resist in Acetone, clean with IPA	30 sec
6.b	Coat PR	Coat SU 8 2010 Resist (-ve resist) Thick coating (18um).	500RPM for 10 sec thn 3000RPM for 60sec
7.b	Bake	Su 8 2010 PEB @ 100 degree celcius (untill the resist flows evenly)	2min
8.b	Expose	Su 8 2010 Expose on Karl Suss	75sec
8.b.1	Bake	Su 8 2010 bake at 100 degree celcius. (can see pattern on resist)	2min
9.b	Develop	Develop the Resist (Su 8 2010) in SU 8 developer.	3min
10.b	PEB	PEB bake at 175 C for SU 8 2010	2min
11	Drill	Drill holes on Substrate-2	NA
12	Seal	Seal the processed substrates using parylene (2um)	NA
6.a	Coat PR	Coat SU 8 2050 Resist (-ve resist) Thick coating (30um).	500RPM for 10 sec thn 4000RPM for 60sec
7.a	Bake	Su 8 2050 PEB @ 100 degree celcius (untill the resist flows evenly)	4min
8.a	Expose	Su 8 2050 Expose on Karl Suss	100sec
8.a.1	Bake	SU 8 2050 bake at 100 degree celcius. (can see lithography pattern)	3min
9.a	Develop	Develop the Resist (Su 8 2050) in SU 8 developer.	5 min
10.a	PEB	PEB bake at 175 C for SU 8 2050	3min

Figure A-2: Process Flow for Parallel Plate Device with SU 8 Resist

Figure A-3 shows the "absolute humidity" in g/m^3 (upper line) and the "dew point temperature" of the air in°C (lower line) for certain air temperatures as a function of "relative humidity.

Relative humidity	10%	20%	30%	40%	50%	60%	70%	80%	90%	100%
Air temperature [°C]										
+50	8.3	16.6	24.9	33.2	41.5	49.8	58.1	66.4	74.7	83.0
	+8	+19	+26	+32	+36	+40	+43	+45	+48	+50
+45	6.5	13.1	19.6	26.2	32.7	39.3	45.8	52.4	58.9	65.4
	+4	+15	+22	+27	+32	+36	+38	+41	+43	+45
+40	5.1	10.2	15.3	20.5	25.6	30.7	35.8	40.9	46.0	51.1
	+1	+11	+18	+23	+27	+30	+33	+36	+38	+40
+35	4.0	7.9	11.9	15.8	19.8	23.8	27.7	31.7	35.6	39.6
	-2	+8	+14	+18	+21	+25	+28	+31	+33	+35
+30	3.0	6.1	9.1	12.1	15.2	18.2	21.3	24.3	27.3	30.4
	-6	+3	+10	+14	+18	+21	+24	+26	+28	+30
+25	2.3	4.6	6.9	9.2	11.5	13.8	16.1	18.4	20.7	23.0
	-8	0	+5	+10	+13	+16	+19	+21	+23	+25
+20	1.7	3.5	5.2	6.9	8.7	10.4	12.1	13.8	15.6	17.3
	-12	-4	+1	+5	+9	+12	+14	+16	+18	+20
+15	1.3	2.6	3.9	5.1	6.4	7.7	9.0	10.3	11.5	12.8
	-16	-7	-3	+1	+4	+7	+9	+11	+13	+15

Absolute humidity (as g/m3)

$$D = \frac{804}{1 + 0.00633t} \times \frac{e}{PO}$$

$$= \frac{H}{100} \times \frac{804}{1 + 0.00366t} \times \frac{e}{PO}$$

H = relative humidity (% RH)
PO = standard air pressure (mm Hg)
D = absolute humidity (g/m^3)
e = water steam pressure (mm Hg)
DS = absolute humidity in saturation (g/m^3)
eS = saturated water steam pressure (mm Hg)
t = temperature (°C)
T = dew point temperature

Figure A-3: Relative Humidity to Absolute Humidity Conversion Chart

The spin speed curves are not repeatable perfectly; especially since we were using substrates that were not standard. The curves below were referred to get an estimate and design process rather than create a complete spin speed curve.

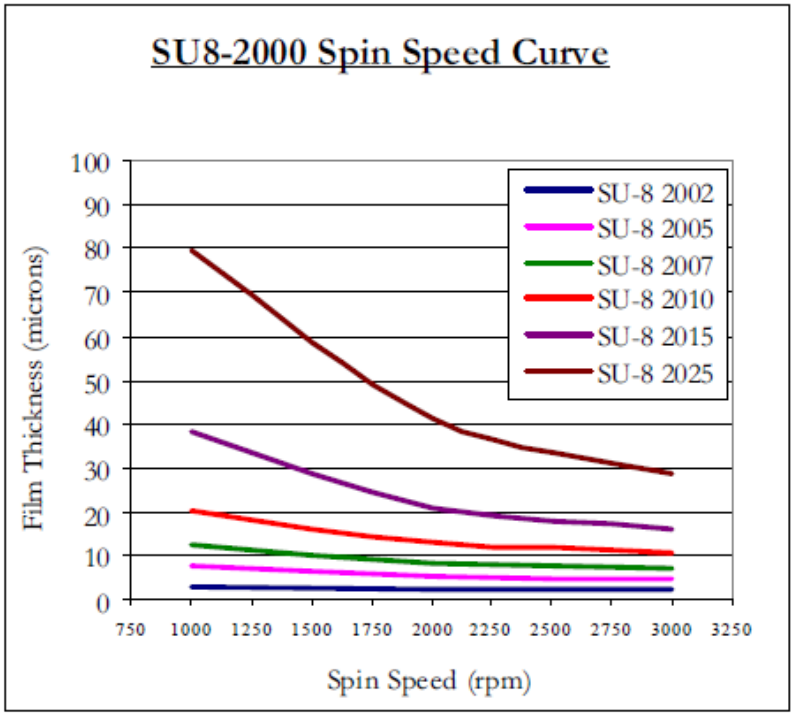

Figure A-4: SU 8 Resist Speed vs. Thickness Plot

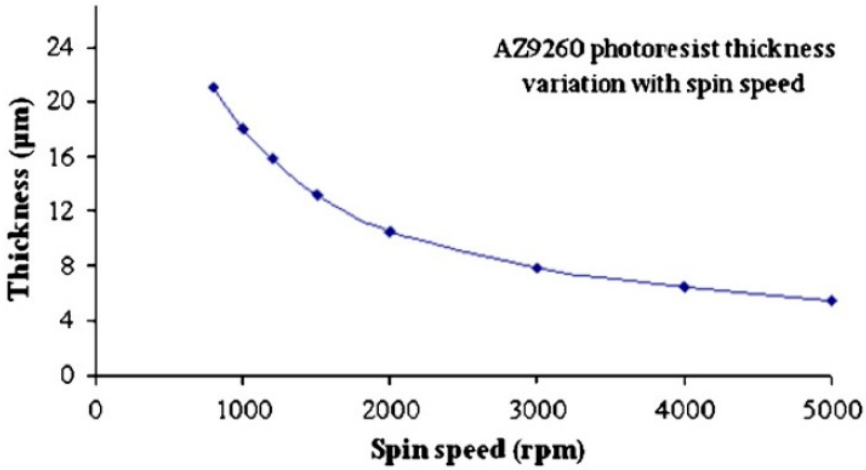

Figure A-5: AZ9260 Resist Speed vs. Thickness Plot